MSc

2.º CICLO

FCUP
ICBAS
2022

Adipose tissue metabolic fingerprints in obesity

Marcelo José Varandas Topete

Adipose tissue metabolic fingerprints in obesity

Marcelo José Varandas Topete

Master`s thesis in Biochemestry presented to
Faculty of Ciences and
School of Medicine and Biomedical Sciences
University of Porto

2022

Adipose tissue metabolic fingerprints in obesity

Marcelo José Varandas Topete
Mestrado em Bioquímica
Departamento de Anatomia, Instituto de Ciências Biomédicas Abel Salazar, Universidade do Porto
2022

Orientadora
Sofia S. Pereira, PhD, Professora Auxiliar, Instituto Ciências Biomédicas Abel Salazar, Universidade do Porto

Co-orientadora
Sara Andrade, PhD, Investigadora, Instituto Ciências Biomédicas Abel Salazar, Universidade do Porto

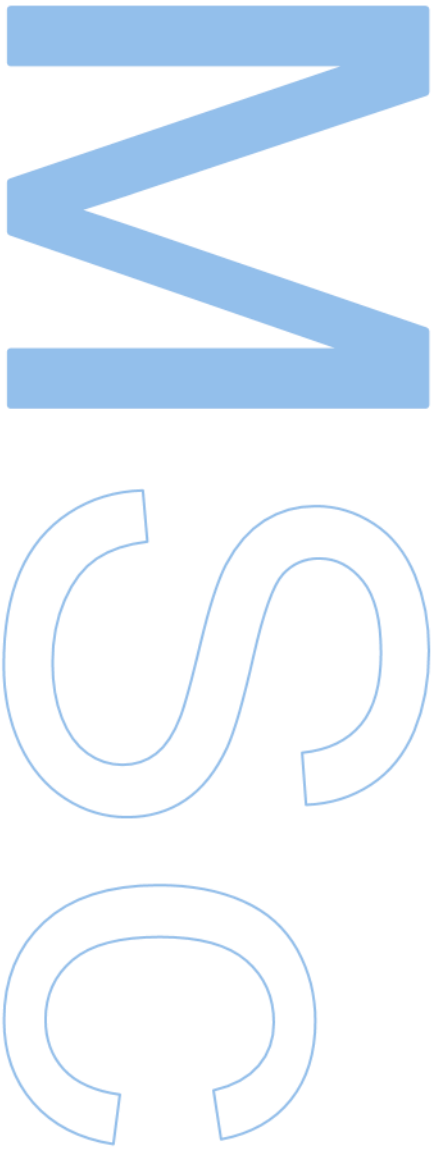

Todas as correções determinadas pelo júri,
e só essas, foram efetuadas.

O Presidente do Júri,

Porto, _____/_____/_____

“Life is not easy for any of us. But what of that? We must have perseverance and, above all, confidence in ourselves. We must believe that we are gifted for something, and that this thing, at whatever cost, must be attained.”

Marie Curie

Declaração de Honra

Eu, Marcelo José Varandas Topete, inscrito no Mestrado em Bioquímica da Faculdade de Ciências e Instituto Ciências Biomédicas Abel Salazar da Universidade do Porto declaro, nos termos do disposto na alínea a) do artigo 14.º do Código Ético de Conduta Académica da U.Porto, que o conteúdo da presente dissertação reflete as perspetivas, o rabalho de investigação e as minhas interpretações no momento da sua entrega.

Ao entregar esta dissertação, declaro, ainda, que a mesma é resultado do meu próprio trabalho de investigação e contém contributos que não foram utilizados previamente noutros trabalhos apresentados a esta ou outra instituição.

Mais declaro que todas as referências a outros autores respeitam escrupulosamente as regras da atribuição, encontrando-se devidamente citadas no corpo do texto e identificadas na secção de referências bibliográficas. Não são divulgados na presente dissertação quaisquer conteúdos cuja reprodução esteja vedada por direitos de autor.

Tenho consciência de que a prática de plágio e auto-plágio constitui um ilícito académico.

Marcelo José Varandas Topete

Porto, 30 de setembro de 2022

Acknowledgements

No final, de mais uma etapa, mais complicada, obviamente que não podia de deixar de agradecer àquelas pessoas que direta e indiretamente, contribuíram para a conclusão deste trabalho.

À minha orientadora Sofia Pereira, primeiro por me terem aceitado como seu aluno para a realização deste trabalho, apesar de ter um horário muito preenchido, mostrou-se muito disponível para ajudar, e acompanhar, ajudou-me a melhorar as minhas capacidades, pela sua simpatia, e pela confiança que demonstrou em mim desde o primeiro dia.

À minha coorientadora Sara Andrade, por ter aceitado participar neste trabalho, pela disponibilidade que mostrou em me ajudar e acompanhar, pela motivação que foi sempre dando para realizar as minhas tarefas.

À Madalena, pela excelente pessoa que é, por ter mostrado sempre disponibilidade para me ajudar, por me ter acolhido da melhor maneira no departamento, e em momentos mais em baixos em que eu estava, ela sempre deu motivação tanto a nível profissional e pessoal.

À Raquel Bernardino, por toda a ajuda que me deu neste trabalho e pela disponibilidade para me explicar algumas técnicas que realizei durante a realização deste trabalho.

À Dra. Mariana Monteiro, agradecer por me ter aceitado na equipa, por manter o contacto com o Hospital de modo a arranjar amostras para o meu trabalho, ajudou-me a subir no meu caminho profissional.

À Dra. Marta Guimarães, Dra. Ana Marta e Dr. Mário Nora do (Hospital São Sebastião de Santa Maria da Feira e Hospital da Luz - Arrábida), por aceitarem a colaboração neste estudo. Sem o seu trabalho este trabalho seria difícil de se realizar.

Aos pacientes que aceitaram participar neste estudo.

À Sofia Oliveira, pela amizade, pela excelente pessoa que é, pela sua alegria, simpatia e confiança que me demonstrou desde o 1º dia, pela sua ajuda, pela sua vontade e determinação em aprender algumas técnicas que realizei no laboratório, e pelos conselhos úteis que me deu, que me ajudaram a melhorar o meu trabalho.

Ao António Gil, por também ter ajudado, pela sua simpatia e pela oportunidade que tive de o conhecer, uma pessoa que vai contribuir muito para a ciência. Um exemplo a seguir.

À Ana, Gil e Patrícia, pela sua simpatia e por me integrado bem no departamento.

Aos Motoristas do ICBAS pela sua disponibilidade em me levar até Santa Maria da Feira de modo que fosse possível recolher as amostras para o estudo.

Aos meus amigos, especialmente ao Alex, Guedes, Gil, Joel e Toni, pelo tempo que perderam para me ouvirem quando estava mais em baixo, por me darem sempre motivação e apoio.

À minha família, por acreditarem sempre em mim e por estarem sempre presentes nos meus bons e maus momentos, e por fazerem todos os esforços para me ajudar/apoiar.

À Fundação para a Ciência e Tecnologia (FCT) pelo financiamento, pois sem este não era possível realizar este projeto de investigação (UIDB/00215/2020, UIDP/00215/2020, LA/P/0064/2020 e PTDC/MEC-CIR/3615/2021).

Resumo

Introdução: A prevalência mundial da obesidade triplicou nas últimas quatro décadas, sendo atualmente um problema de saúde pública. O tecido adiposo desempenha um papel central na manutenção da homeostase energética. Na obesidade, o tecido adiposo sofre uma remodelação complexa, particularmente na composição celular relativa e no metabolismo energético. Até agora ainda não se sabe se essa reprogramação metabólica é semelhante em diferentes classes de obesidade.

Objetivos: Avaliar a função bioenergética e a preferência do tecido adiposo visceral (VAT) para diferentes substratos energéticos, em indivíduos com diferentes índices de massa corporal (IMC): IMC< 40 kg/m^2 e IMC ≥ 40 kg/m^2.

Métodos: Fragmentos de VAT obtidos de pacientes (n=15) com um IMC entre 35 e 40 kg/m^2 (n=7) e ≥40 kg/m^2 (n=8), foram colhidos durante a cirurgia bariátrica. A função bioenergética do VAT e a seu substrato energético preferencial foi avaliado através da incubação do VAT com um inibidor do transportador do piruvato (UK5099), um inibidor da glutaminase (BPTES) e o inibidor da carnitina palmitoiltransferase-1 (Etomoxir), utilizando a tecnologia Seahorse. A expressão de genes relacionados com o metabolismo da glicose/piruvato, da glutamina e dos ácidos gordos foi quantificada usando o qRT-PCR.

Principais resultados: Em condições basais, o consumo de oxigénio não-mitocondrial foi maior no VAT dos pacientes com IMC ≥40 kg/m^2 quando comparado com os dos pacientes com IMC <40 kg/m^2 (0.04 ± 0.01 µg/min/µg/mL de proteína total vs 0.02 ± 0.002 ρmol/min/µg/mL de proteína total, p<0.05). O piruvato é o substrato energético mitocondrial preferencial do VAT, independentemente da categoria de IMC dos pacientes. No VAT de pacientes com IMC <40 kg/m2, a combinação do UK5099 e do BPTES levou a uma diminuição significativa da percentagem de respiração máxima (43.94 ± 10.49 % vs 100.00 ± 39.57 %, p<0.05); da capacidade respiratória de reserva (49.81 ± 24.17 % vs 100.00 ± 30.62 %, p<0.05); enquanto a combinação do UK5099 com o Etomoxir levou ao aumento significativo do *proton leak* (355.50 ± 131.90 % vs 100.00 ± 28.55 %, p<0.01). Nenhum dos inibidores usados influencio significativamente a função bioenergética do VAT de pacientes com o IMC ≥40 kg/m^2. Além disso, a expressão dos genes estudados era semelhante entre os dois grupos de estudo.

Conclusão: O piruvato é o substrato mitocondrial preferencial do VAT de pacientes com obesidade. A glutamina aumentou o *proton leak* no VAT de pacientes com um IMC <40 kg/m^2, parecendo, portanto, ter um papel protetor contra a produção

de espécies reativas de oxigénio (ROS). Este mecanismo parece não existir no VAT de pacientes com obesidade mórbida. Assim, as estratégias de tratamento da obesidade baseadas na modulação da disponibilidade de substrato, são possivelmente mais promissoras em pacientes com um IMC <40 kg/m^2.

Palavras-chave: Obesidade, Tecido adiposo visceral, Disfunção mitocondrial, Piruvato, Glutamina, Ácidos Gordos

Abstract

Introduction: The worldwide prevalence of obesity has tripled in the last four decades, becoming a major public health problem. Adipose tissue plays a central role in maintaining energy homeostasis. In obesity, adipose tissue undergoes complex remodeling, particularly in relative cellular composition and energy metabolism. Whether this metabolic reprogramming is similar across different obesity classes is still unknown.

Objectives: To compare the bioenergetic function and energy substrate preference of visceral adipose tissue (VAT) pertaining to individuals with obesity with different body mass indexes (BMI): BMI< 40 kg/m^2 and BMI ≥ 40 kg/m^2.

Methods: VAT fragments from patients (n=15) with a BMI between 35 and 40 kg/m^2 (n=7), and ≥40 kg/m^2 (n=8), were collected during bariatric surgery. VAT bioenergetics and mitochondrial energy substrate preferences were assessed after incubation with a pyruvate carrier inhibitor (UK5099), a glutaminase inhibitor (BPTES) and a carnitine palmitoyltransferase-1 inhibitor (Etomoxir) using the Seahorse® analyzer. Expression of genes related to glucose/pyruvate, glutamine, and fatty acids metabolism was quantified by qRT-PCR.

Results: Under basal conditions, non-mitochondrial oxygen consumption was higher in the VAT of patients with BMI ≥40 kg/m^2 of when compared to those of patients with BMI <40 kg/m^2 (0.04 ± 0.01 ρmol/min/μg/mL of total protein vs 0.02 ± 0.002 ρmol/min/μg/mL of total protein, p <0.05). Pyruvate is the preferred mitochondrial energy substrate used by VAT, regardless the subjects` BMI category. In VAT of patients with a BMI <40 kg/m^2, UK5099 in combination with BPTES significantly decreased the maximum respiration and the spare respiratory capacity (maximum respiration: 43.94 ± 10.49 % vs. 100.00 ± 39.57 %, p<0.05; spare respiratory capacity: 49.81 ± 24.17 % vs. 100.00 ± 30.62 %, p<0.05); while UK5099 in combination with Etomoxir increased the proton leak (355.50 ± 131.90 % vs. 100.00 ± 28.55 %, p<0.01). In VAT of patients with BMI ≥40 kg/m^2, none of the inhibitors influenced any bioenergetic parameter. There were no significant differences in the expression of genes related to metabolism between the groups.

Conclusion: Pyruvate is the preferred mitochondrial substrate of VAT pertaining to patients with obesity. In VAT of patients with a BMI <40 kg/m^2, glutamine by increasing the proton leak, seems to have a protective role against the ROS production, a mechanism that appears to be absent in VAT of patients with more severe obesity. So,

obesity treatment strategies based on substrate availability modulation, are likely to be more promising in patients with a BMI <40 kg/m^2.

Keywords: Obesity, White Adipose Tissue, Mitochondrial Dysfunction, Pyruvate, Glutamine, Fatty Acids

Index

Index of Tables

Index of Figures

Abbreviations

ASP – Acylation Stimulating Protein

ATP – Adenosine triphosphate

ADP – Adenosine diphosphate

BMI – Body Mass Index

BAT - Brown adipose tissue

BPTES - Bis-2-(5-phenylacetamide-1,3,4-thiadiazol-2-yl) ethyl sulfide

FCCP - Carbonyl cyanide-p-trifluoromethoxyphenylhydrazone

CPT1a – Carnitine Palmitoyl transferase 1a

cDNA - complementary Deoxyribonucleic Acid

cAMP - cyclic Adenosine monophosphate

DMSO – Dimethyl Sulfoxide

ETC – Electron Transport Chain

FABP4 – Fatty acid-binding protein 4

NF-kB - Factor nuclear kappa B

FFA – Free Fatty Acids

GIP - Gastric Inhibitory peptide

GLP-1 - Glucagon-like peptide 1

GLS1 – Glutaminase 1

HDL - High-density Lipoprotein

IGF-1 – Insulin like growth factor 1

IFNγ – Interferon-gamma

IL-6 – interleukin-6

VLDL – Very low-density lipoproteins

MHO - Metabolically healthy obesity

MPC1 – Mitochondrial Pyruvate Carrier 1

UK5099 – Mitochondrial Pyruvate Carrier Inhibitor

OCR – Oxygen Consumption Rate

PPAR-γ - Peroxisome proliferator- activated receptor gamma

qRT-PCR - Quantitative Real-Time Polymerase Chain Reaction

ROS - Reactive oxygen species

SAT - Subcutaneous adipose tissue

TCA- Tricarboxylic Acid

TNF-α – Tumor necrosis factor α

T2D – Type 2 diabetes

UCP1 - Uncoupling protein 1

UCP2 - Uncoupling protein 2

UCP3 - Uncoupling protein 3

MUHO - Unhealthy metabolic obesity

VEGF – Vascular endothelial growth factor

VAT - Visceral adipose tissue

WHO – World Health Organization

1 Introduction

1.1 Obesity

Chronic caloric overload, with excess consumption of lipids and carbohydrates, can have a negative impact on non-communicable diseases, such as obesity, Type 2 diabetes (T2D), dyslipidemia and hypertension (Oshio et al., 2020). Although, obesity is a complex, polygenic and multifactorial disease (Mancini & de Melo, 2017), The driver is the imbalance between the energy consumed (food intake) and expended (physical activity) which can be caused by several factors (Figure 1) (Blüher, 2019; Sharma & Padwal, 2010).

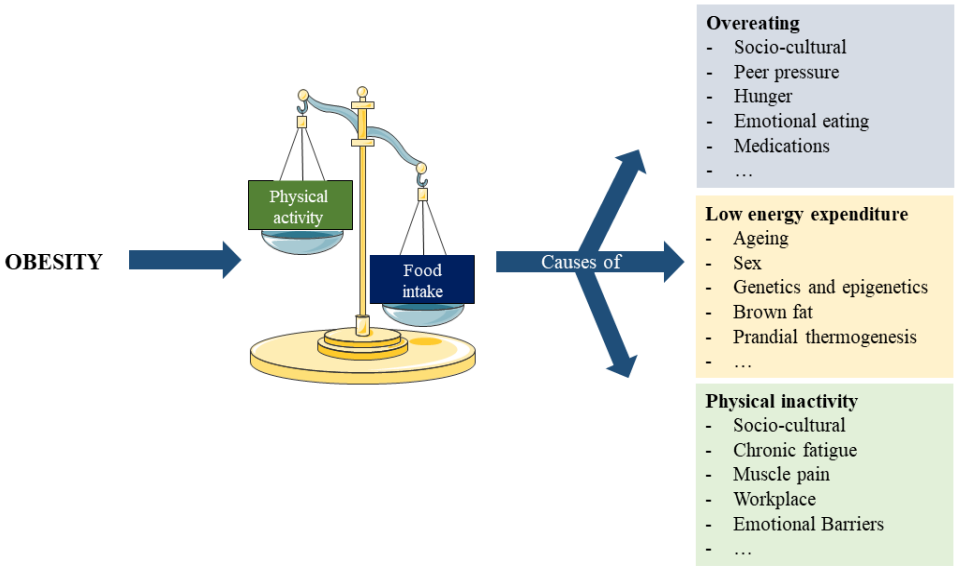

Figure 1 – Causes of obesity. Obesity is caused by an imbalance between energy ingested (food intake) and expended (physical activity). Adapted from (Blüher, 2019; Sharma & Padwal, 2010)

In a simplistic approach, obesity can be diagnosed by the calculation of the body mass index (BMI), which is the ratio between body weight in kilograms and height in square meters (kg/m^2). This index allows to classify the patients according to different risk categories and it is an easy tool to monitor adiposity changes over time, both at individual and population levels (Table 1) (Piché, Tchernof, & Després, 2020). According to the World Health Organization (WHO), obesity can be defined by a BMI greater than 30 kg/m^2. In addition, this disease can be divided into four severity categories, where individuals who present a BMI in the range of 30-34.9 kg/m^2 are considered to belong to class I; between 35-39.9 kg/m^2 to class II; between 40.0-49.9 kg/m^2 to class III, and a BMI greater than 50 kg/m^2 to class IV (Fernández-Sánchez et al., 2011). In 2015, data from the Global Burden of Disease Obesity Collaborators showed

that over 603.7 million adult individuals had obesity and that 4 million people died due to this disease (Afshin et al., 2017; Piché et al., 2020).

Table 1 - Body Mass Index (BMI) categories**.** Adapted from (Tchernof & Després, 2013)

.

Classification	BMI (Kg/m^2)
Under Weight	≤ 18,5
Healthy Weight	18.5 – 24.9
Overweight	25.0 – 29.9
Obesity – Class I	30.0 – 34.9
Obesity – Class II	35.0 – 39.9
Severe Obesity – Class III	40.0 – 49.9
Severe Obesity – Class IV	≥ 50.0

Obesity is a risk factor for the onset of several other diseases, such as cardiovascular diseases, hypertension, cancer, and T2D (Blüher, 2019). Keaver *et al* estimated that overweight and obesity prevalence can reach 89% of men and 85% of women, in 2030. This will lead to an increase in the prevalence of coronary heart disease by 97%, cancers by 61%, and T2D by 21%, having a huge impact on the health care systems. It is estimated that a 5% of BMI reduction would reduce healthcare spending in about 495 million euros (Engin, 2017).

The failure of health care systems to treat obesity at early stages can lead to the progression to more severe stages. Many health care systems and insurance companies do not recognize obesity as a chronic progressive disease, causing a delay in the obesity treatment through more efficient approaches. This postponement can cause a self-perpetuating progression of the disease, such as further weight gain, and reduced physical activity, which can have a psychological effect and consequently driving the vicious cycle of body weight gain (Blüher, 2019).

Obesity treatment strategies include lifestyle interventions, pharmacotherapy, and bariatric surgery. Severe obesity is recognized for being refractory to lifestyle and pharmacological treatment, while bariatric surgery is the only intervention with proven efficacy to achieve significant and sustained weight loss (Adams et al., 2017).

1.2 Adipose Tissue

The adipose tissue is one of the largest organs in the body. It represents about 20 to 28% of body mass in healthy people. However, this percentage varies according to gender and metabolism. In individuals with obesity, it can even represent 80% of the body mass. Adipose tissue consists of adipocytes, a vascular fraction of blood and lymphatic vessels, that includes endothelial cells, smooth muscle cells, and a matrix that includes collagen, immune cells, adipocyte precursor cells (pre-adipocytes), and mesenchymal stem cells (Frigolet & Gutiérrez-Aguilar, 2020; Heinonen, Jokinen, Rissanen, & Pietiläinen, 2020).

One of the main functions of adipose tissue is the storage of excess calories in the form of triglycerides from which free fatty acids are released during fasting, to prevent energy shortage. In the post-absorptive phase, glucose is captured from the bloodstream into the adipocytes producing glycerol-3-phosphate (via glycolysis), an essential substrate for lipogenesis. Lipids obtained from the diet are moved from the intestine to the liver via chylomicrons, to be esterified into glycerol-3-phosphate. These esterified fatty acids are then transported by the very low-density lipoproteins (VLDL) to the adipose tissue (Figure 2) (Berg, 2012; Coelho et al., 2013; David L. Nelson, 2014; Unamuno, Frühbeck, & Catalán, 2019). In the adipocytes, glucose metabolism and lipogenesis leads to the production of malonyl-CoA, which inhibits the import of fatty acids into the mitochondria via the transporter Carnitine Palmitoyl Transferase 1 (CPT1), thus decreasing fatty acid oxidation. Conversely, in a state of energy deprivation, there is the activation of the AMPK, which decreases malonyl-CoA and leading to increased CPT1 activity and β-oxidation (Heinonen et al., 2020).

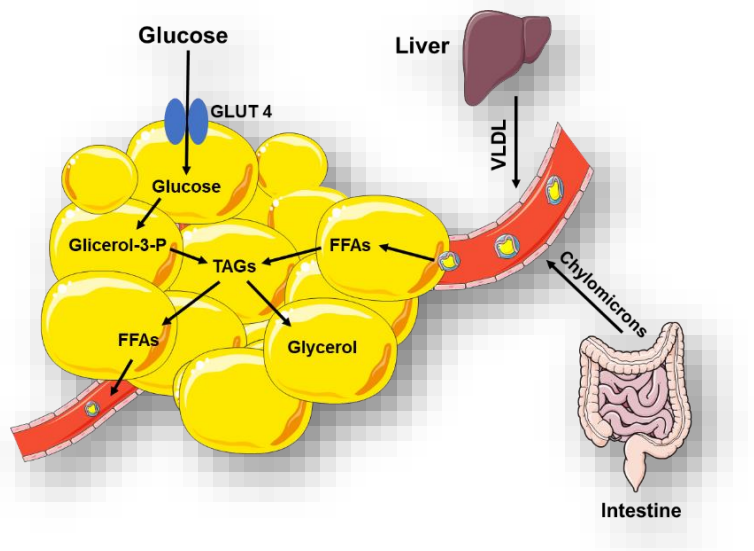

Figure 2 – Principal metabolic role of adipose tissue. During the post-absorptive state, insulin production by the pancreatic β-cells will activate its receptors in the adipose tissue and peripheral organs causing translocation of GLUT4 to the membrane. Glucose is stored, in the adipose tissue, in the form of triglycerides (TAGs). Lipids absorbed in the intestine are transported to the liver via chylomicrons, to be esterified into free fatty acids (FFAs). Those are transported to the adipose tissue and stored as TAGs. Adapted from (Coelho, Oliveira, & Fernandes, 2013)

1.2.1 Types of Adipose Tissue

There are three different histological types of adipose tissue (white, brown and beige) which vary, according to its functions, color, vascularization, and structure (Figure 3). White adipose tissue (WAT) is the most abundant type, and it is characterized by its white color and sparse vascularization compared to brown tissue (BAT). It can be found in various anatomical locations, such as in subcutaneous deposits - located below the skin and in visceral deposits - in the intra-abdominal region and the cardiac region. The subcutaneous adipose tissue (SAT) is a less inflammatory adipose tissue and it is more susceptible to acquire BAT characteristics comparing to visceral adipose tissue (VAT) (Fenzl & Kiefer, 2014; Frigolet &

Gutiérrez-Aguilar, 2020; van Dam, Boon, Berbée, Rensen, & van Harmelen, 2017; Vidal & Stanford, 2020). VAT is also an endocrine organ, since it is able to produce adipokines that regulate energy intake and expenditure, body weight, glucose and lipid metabolism, insulin sensitivity, pre-adipocyte generation, and cell migration in adipose tissue (Table 2) (Coelho et al., 2013).

Table 2 - Regulation and function of hormones secreted by adipose tissue.

Molecule	Function/Effect
Adiponectin	Plays a protective role in the pathogenesis of type 2 diabetes and cardiovascular diseases
Adipsin	Potencial relation between between the complemente pathway and adipose tissue metabolism. Decreased inflammation by clearance of dead cells. Increased inflammation by chemotaxis
ASP	Influences the rate of triacylglycerol synthesis in adipose tissue
FABP4	Is increased by obesity. Increased gluconeogenesis, insulin resistance and atherogenesis
FFA	Oxidized in tissues to produce local Energy. Serve as a substrate for triglyceride and structural molecular synthesis. Involved in the development of insulin resistance.
Glycerol	Structural componente of the major classes of biological lipids and gluconeogenic precursor
IGF-1	Stimulates proliferation of a wide variety of cells and mediates many cells and many of the effects of growth hormone
IL-6	Increased by inflammatory cytokines, lipolysis and obesity. Pro-inflammatory, lipid and glucose metabolism, regulation of body weight Increased hepatic gluconeogenesis
Leptin	Regulation of apetite and Energy expenditure.
Resistin	Is increased by inflammation. Increased insulin resistance and inflammation
TNF-α	Affects insulin receptor signaling, may lead to development of insulin resistance in obesity
Vapsin	Is increased by obesity, and decreased insulin resistance
VEGF	Stimulation of angiogenesis

Adapted from (Coelho et al., 2013; Scheja & Heeren, 2019)**; FABP4** – fatty acid-binding protein 4; **TNF-α** – tumor necrosis factor α, **IL-6** – interleukin-6; **ASP** – acylation stimulating protein; **VEGF** – vascular endothelial growth factor; **IGF-1** – insulin like growth factor 1; **FFA** – free fatty acids

Brown adipose tissue (BAT) is mainly located in supraclavicular, cervical and paravertebral fat deposits. Compared to WAT, BAT is more a vascularized tissue, and it has a higher content of mitochondria, with high oxidative capacity (Chondronikola, 2020; Fenzl & Kiefer, 2014; Frigolet & Gutiérrez-Aguilar, 2020). Unlike WAT, in BAT, lipids are the fuel source for oxidative phosphorylation and consequently for heat production. A characteristic feature of BAT is the presence of high levels of the uncoupling protein 1 (UCP1), a key protein for thermogenesis (Betz & Enerbäck, 2018; David L. Nelson, 2014; Fenzl & Kiefer, 2014). When thermogenesis is activated, BAT deposits increase through hypertrophic and hyperplastic processes (Villarroya, Cereijo, Villarroya, & Giralt, 2017).

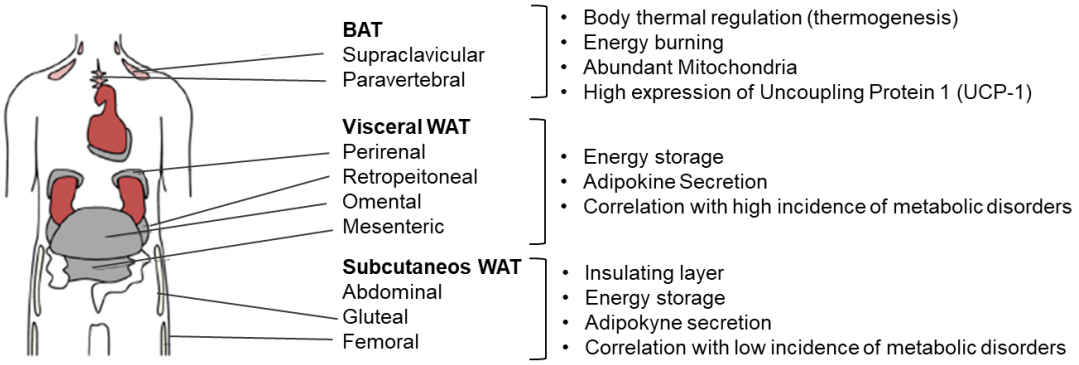

Figure 3 - Location of the different types of adipose tissue and mechanisms associated, adapted from (Choe, Huh, Hwang, Kim, & Kim, 2016).

The beige adipose tissue has a similar appearance to BAT (Pilkington, Paz, & Wankhade, 2021). Beige adipocytes have multilocular lipid droplets, a central nucleus, and a high density of mitochondria. It also generates energy in the form of heat, contributing to thermogenesis. Beige adipose tissue exhibits high plasticity because when there is no cold exposure, UCP1 expression and mitochondrial content decreases, leading to the transition from beige adipocytes to a white adipocyte phenotype (Ikeda, Maretich, & Kajimura, 2018). Although the knowledge available for this adipose tissue type is more scarce, there was a recent increase in the number of studies focused on beige adipose tissue in order to understand possible mechanisms involved in transition between WAT to BAT in an attempt to identify targets to be used therapeutic approaches for obesity or other metabolic diseases (Ikeda et al., 2018).

1.2.2 White adipose tissue in obesity

In energy surplus conditions, the WAT expands by increasing its volume (hypertrophy) or increasing the number of adipocytes, through *de novo* adipogenesis (hyperplasia) (Scheja & Heeren, 2019). This expansion through hypertrophy or hyperplasia is a well-known characteristic of the adipose tissue of individuals with overweight or obesity. When hypertrophy is dysfunctional or excessive, the WAT undergoes structural and cellular changes such as local inflammation, infiltration of immune cells, cell death, insulin resistance, and impaired metabolism. These adipocytes become insulin resistant, lose the ability to properly store triglycerides, and have an impaired energy expenditure. Subsequently, the fatty acids are released into the circulation and accumulate in other organs, leading to cellular stress and metabolism dysfunction, similar to what happens in metabolic diseases, such as T2D (Figure 4) (Heinonen et al., 2020; Scheja & Heeren, 2019). Adipose tissue hyperplasia is related to the increase on pre-adipocytes and adipocytes number, and it was described

has having a preventing role on insulin resistance, or ectopic lipid accumulation (Figure 4) *(Hepler & Gupta, 2017; Jang et al., 2016; White & Ravussin, 2019).*

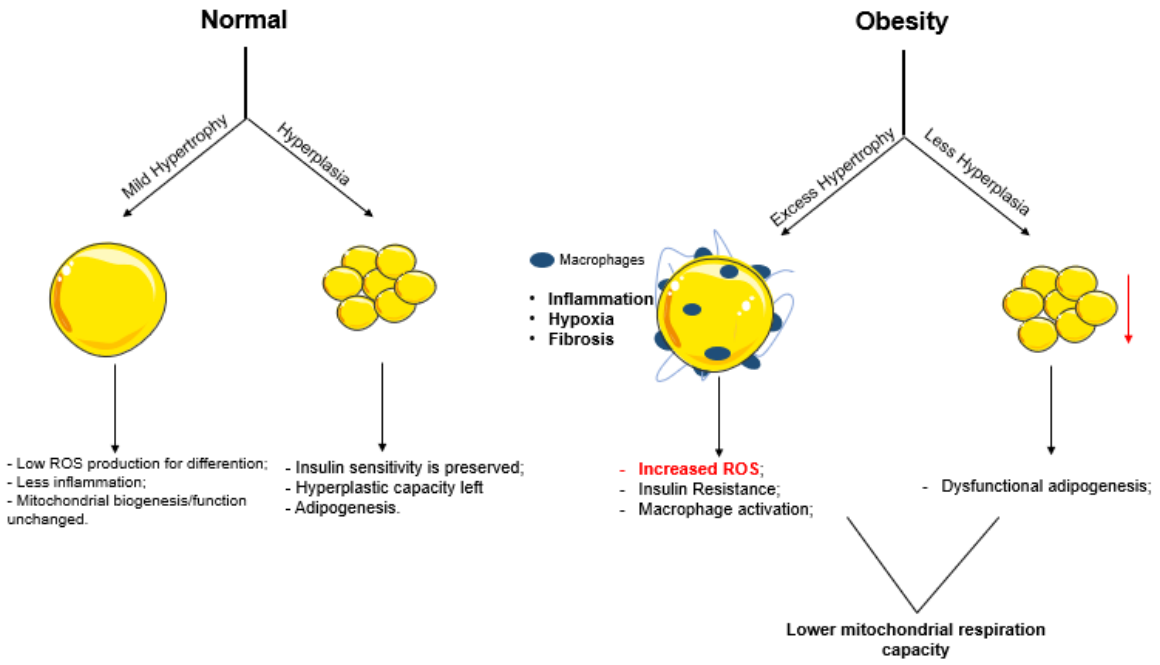

Figure 4 – White Adipose Tissue Expansion in Obesity. In obesity, adipocytes hypertrophy is associated with inflammation, hypoxia, fibrosis, and insulin resistance. As consequence of lipid overflow, ectopic lipid accumulation and lipotoxicity occurs. On the other hand, the hyperplasia of adipose tissue delays or prevents insulin resistance or ectopic lipid accumulation. Adapted from (Hepler & Gupta, 2017).

1.3 Adipocytes mitochondrial dysfunction in obesity

Mitochondria are the main source of Adenosine triphosphate (ATP) in cells. In addition to this function, mitochondria have other important functions in the cell, such as the production of metabolites required for cytosolic processes, amino acid catabolism, ketogenesis, urea cycle, formation of reactive oxygen species (ROS), calcium cycling and regulation of a variety of cell signaling pathways, including key roles as effectors of apoptosis and cell death (Boudina & Graham, 2014).

Structurally, mitochondria are divided into four components: 1) outer membrane, where the ions are freely transported, as well as small molecules; 2) intramembrane space, where the accumulated protons create an electrochemical gradient; 3) inner membrane, where phosphate, ADP, ATP, and subunits of the mitochondrial complexes are transported and 4) matrix where the oxidation of pyruvate and fatty acids occur (Fig.1). Mitochondria can change its number, size, and activity within a cell by altering mitochondrial dynamics through biogenesis, fusion, and fission. Peroxisome proliferator-activated receptor gamma

coactivator-1 alpha (PGC1-α) is one of the coactivators of this dynamics, activating various genes in oxidative phosphorylation, adaptive thermogenesis, fatty acid oxidation, glucose uptake, and others. Maintenance of mitochondrial function and repair depends on fusion, fission, and autophagy. These are unique features that make mitochondria an organelle with complex actions in energy metabolism, as well as in cell fate (Kwak, Park, Lee, & Lee, 2010).

An imbalance between the nutritional substrates availability, the energy production and the oxidative respiration, results in mitochondrial dysfunction. Although adipocytes contained in the WAT have a small mitochondrial density, mitochondria play an essential role for many different pathways in the adipocyte (Kusminski & Scherer, 2012) .

Mitochondrial dysfunction impacts adipocyte dynamics by altering the adipogenesis, the adipocyte lipogenic and lipolytic pathway and by decreasing the production and release of important adipokines involved in lipid homeostasis, the adiponectin (Kusminski & Scherer, 2012).

In the adipocytes of individuals with obesity, mitochondria have less capacity to produce ATP, the inner membranes are less defined (Hernández-Aguilera et al., 2013), the fatty acid oxidation is also reduced and there is a higher glucose dependence for ATP synthesis comparing with individuals without obesity (de Mello, Costa, Engel, & Rezin, 2018; Kusminski & Scherer, 2012; Rogge, 2009). The excessive nutrient intake of these individuals is also related to the induction of inflammatory cascades in WAT. When there is a higher concentration of nutrients, there is a mitochondrial overload of fatty acids and glucose, leading to a higher production of Acetyl-CoA, and so a higher availability of electrons to the complexes of the mitochondrial respiratory chain which contributes to a higher production of ROS. This increase ROS production induce oxidative stress and so the activation of the transcription factors involved in the inflammatory response, such as the nuclear factor kappa B (NF-κB) will be activated (Bournat & Brown, 2010; de Mello et al., 2018; Muñoz & Costa, 2013).

Several studies have found that ROS may be important in adipocyte differentiation and that mitochondrial biogenesis increases during adipocyte differentiation (Lu, Ji, Chang, Su, & Yang, 2010; Wilson-Fritch et al., 2003; Zhang, Marsboom, Toth, & Rehman, 2013). The expansion of mitochondrial content leads to higher metabolic rates in order to overcome the energy requirements for adipocyte differentiation. Differentiation is associated with superoxide production by complex III, conversion of superoxide to hydrogen peroxide, and activation of the transcriptional machinery for adipogenesis (Masschelin, Cox, Chernis, & Hartig, 2020; Tormos et al., 2011). ROS in differentiating cells correlates with increased binding of factor C/EBPβ to DNA and acceleration of clonal mitotic expansion. (Kim, Tang,

Li, & Lane, 2007; Lee, Lee, Choi, Ko, & Kim, 2009). In obesity, the accumulation of ROS restricts the mitochondrial biogenesis and consequently the adipocyte differentiation (Masschelin et al., 2020).

In addition, prolonged oxidative stress can alter the activity of enzymes involved in the Krebs cycle and in the electron transport chain (ETC). Mitochondrial aconitase, the enzyme that converts citrate to isocitrate in the tri-carboxylic acid (TCA) cycle, is one of the protein targets of ROS. Previous studies found that, the superoxide radical inhibits the aconitase leading to a decrease on the TCA cycle intermediates levels and consequently to a decrease on the generation of NADH and FADH2 that are used as electron carriers in the ETC (Armstrong, Whiteman, Yang, & Jones, 2004; Gardner, Raineri, Epstein, & White, 1995; Hausladen & Fridovich, 1994; Lushchak, Piroddi, Galli, & Lushchak, 2014). This mechanism works as an antioxidant defense mechanism, since a smaller electron transport through the ETC decreases the production of ROS (Scandroglio, Tórtora, Radi, & Castro, 2014). In addition, ROS also slow the β-oxidation and inactivate the pyruvate dehydrogenase inhibitor (PDHK2). Pyruvate dehydrogenase activation and aconitase inactivation leads to the export of citrate to the cytosol for fatty acid synthesis (Hurd et al., 2012).

Cells mitochondrial metabolism is oxygen dependent. In the WAT of individuals with obesity, the adipocytes enlargement leads to oxygen deprivation. Some studies found that oxygen consumption of adipose tissue is reduced in obesity, resulting in a lower mitochondrial oxidative metabolism. In addition, other studies found that hypoxia is one of the mechanisms involved in the in chronic low-grade inflammation observed in patients with obesity (Heinonen et al., 2020; Khanna, Khanna, Khanna, Kahar, & Patel, 2022; O'Rourke et al., 2011).

In addition, there is an increase in lipid peroxidation in VAT of individuals with obesity, due to the high levels of fatty acids, which can lead to mitochondrial membrane damage. The peroxidation of polyunsaturated fatty acids also results in the release of diffusible reactive lipid aldehydes, which may impair the function of zinc finger-containing transcription factors, histones and other nuclear proteins in VAT (Hauck et al., 2018; Kowaltowski & Vercesi, 1999; Masschelin et al., 2020).

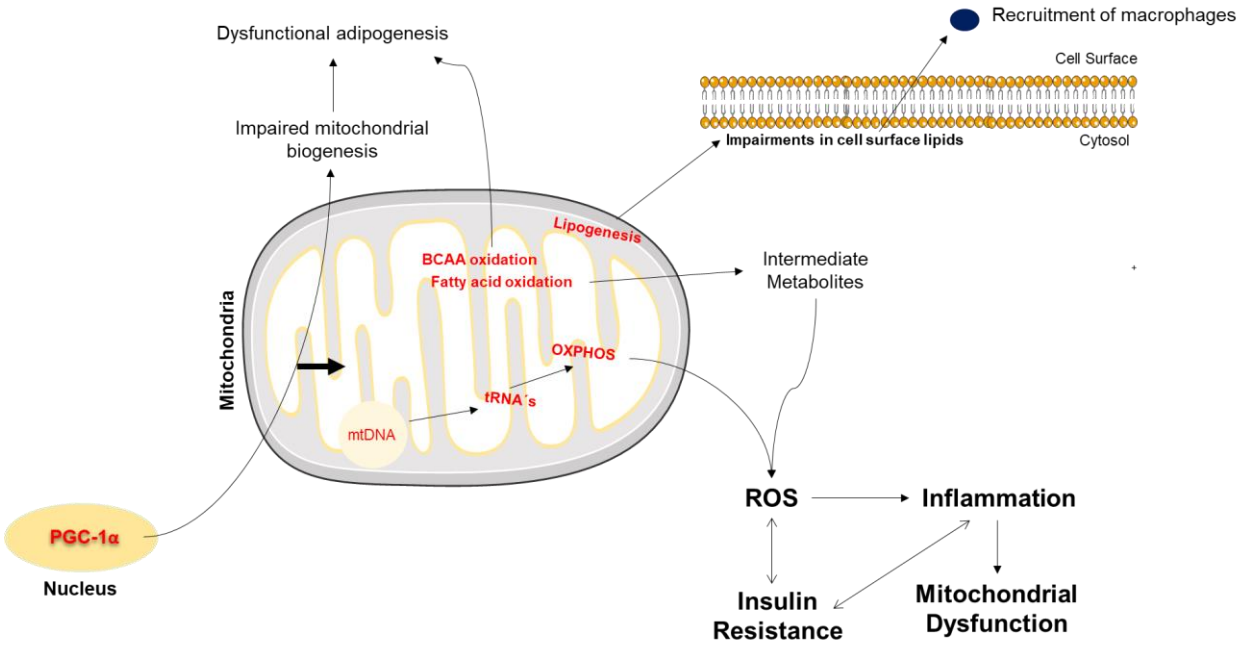

Figure 5 – Mitochondrial dysfunction in obesity. In obesity, PGC-1α is downregulated and affects mitochondrial biogenesis, adipogenesis and expression of mitochondrial genes, such as OXPHOS genes. Increased ROS production can lead to increased insulin resistance, macrophage recruitment and consequent inflammation. In case of impaired of mitochondrial biogenesis, lipogenesis is affected leading to the generation of phospholipids that can induce the infiltration of inflammatory cells. ROS – Reactive oxygen species; BCAA - Branched Chain Amino Acid; PGC-1α - Peroxisome proliferator-activated receptor gamma coactivator 1-alpha. Adapted from (Heinonen et al., 2020).

Although mitochondrial dysfunction has been well documented in WAT of individuals with obesity when compared with normal weight individuals, how does WAT mitochondrial function behave in individuals across different classes of obesity is still poorly understood.

2 Aim

This work aim was to compare the bioenergetic function and the preference in subtract use by the VAT of patients with distinct obesity classes, namely BMI < 40 kg/m^2 and BMI ≥ 40 kg/m^2, in order to understand whether metabolic reprogramming could be contributing to the progression of the disease.

3 Material and methods

3.1 Subjects and samples collection

After approval by the Local Ethics Committee of Centro Hospitalar de Entre Douro e Vouga E.P.E (CA 0830/16-Ot) and Hospital da Luz Arrábida (CA-0032/2022-0T_MP/CC), patients planning to undergo bariatric surgery for the primary treatment of obesity were invited to participate in this study. Patients with T2D a condition known to be associated with mitochondrial dysfunction, history of neoplastic disease or a previous bariatric surgery were excluded from the study. Patients that accepted to participate in this study, signed an informed consent form before surgery. In addition, all procedures were conducted in accordance with the Local, National and European Ethical Guidelines for Medical Research involving Human Subjects.

During bariatric surgery, patients enrolled (n=21) had a visceral adipose tissue (VAT) sample collected under sterile conditions. Among these, those whose VAT did not depict to present satisfactory vitality during the bioenergetic assays (no oxygen consumption or no response to the mitochondrial modulators) (n=6) were excluded from data analysis.

After collection, a VAT fragment was stored at -80 ºC for later RNA extraction, and the remaining was divided into 21 fragments with approximately 5 mg for bioenergetic analyses.

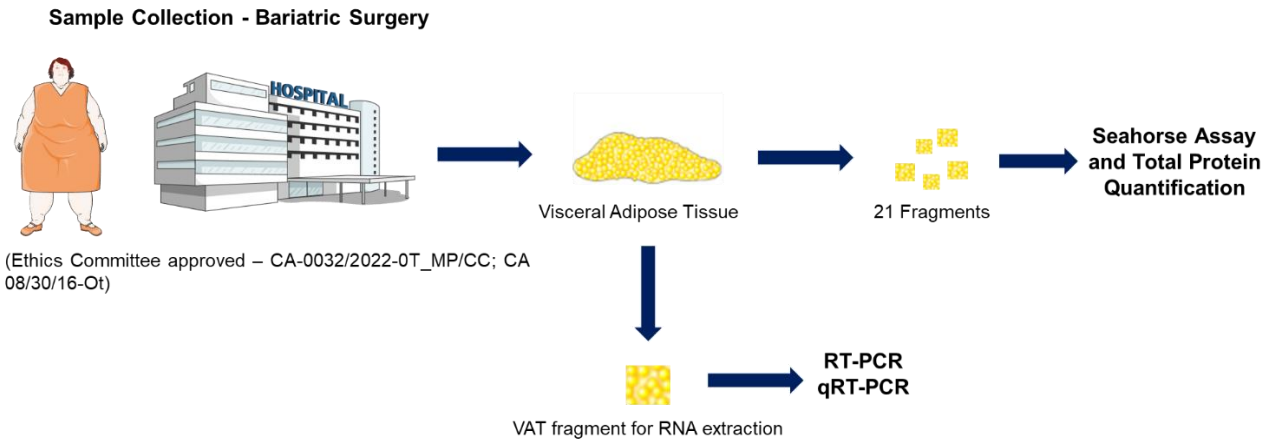

Figure 6 - Schematic representation of VAT collection and initial processing. RT-PCR – Reverse Transcription Polymerase Chain Reaction; qRT-PCR – quantitative Real Time Polymerase Chain Reaction.

3.2 Gene expression analysis

3.2.1 RNA isolation and quantification

Total RNA was extracted from the VAT fragments using the RNeasy® Lipid Tissue kit (74804, QIAGEN, Germany), following the manufacturer instructions.

Briefly, approximately 100 mg of VAT was homogenized in the lysis reagent using the TissueRuptor® (QIAGEN, Germany). After tissue homogenization, the homogenate was

incubated for 5 minutes, at room temperature. Then chloroform was added, stirred vigorously for 15 seconds, and rested for 3 minutes, at room temperature. The samples were then centrifuged for 15 minutes at 12,000g at 4°C, allowing the separation of the aqueous and the organic phases. At the end of the centrifugation, the aqueous phase was transferred to a new tube, and the organic phase was discarded. To the aqueous phase, 70% ethanol was added. The samples were applied to RNase Mini Spin column, that allowed total RNA purification. After RNA purification, it was recovered in RNase Free Water. Total RNA was quantified using a BioTek® SYNERGY^{H1} microplate reader (BioTek®, Agilent Instruments, USA) with a Gen5™ Data Analysis Software (BioTek®, Agilent Instruments, USA).

3.2.2 Synthesis of cDNA

cDNA synthesis was achieved using the Maxima First Strand cDNA Synthesis Kit with double-strand specific DNase (dsDNase) (K1671, Thermo Fisher Scientific Inc, USA). Briefly, for DNA genomic removal, 250 ng RNA was incubated for 2 minutes, with dsDNAses. After that, the 5x Reaction Mix and the Maxima Enzyme Mix was added, for a total of 10 µL. A mixture without the reverse transcriptase (RT) enzyme was performed and will be called “RT – control”. The mixtures were then incubated in a T100™ Thermal Cycler (Bio-Rad, USA) using the following program: 10 minutes at 25 ºC followed by 15 minutes at 50 ºC and 5 minutes at 85 ºC.

3.2.3 Conventional PCR for amplification of genes involved glucose, lipid, and glutamine metabolism

The primers for RNA Polymerase II (*RPII*) , *β-actin* (Mehta et al., 2010), leptin (*ob*) (Liu et al., 2003), GLUT 4 (*SLC2A4*) (Suchacki et al., 2020), mitochondrial pyruvate carrier 1 (*MPC1*) (Wang et al., 2016), Neutral amino acid transporter (*SLC1A5*) (Yoo et al., 2020), glutaminase 1 (*GLS1*) (Yu et al., 2015) and Carnitine palmitoyl-transferase 1a (*CPT1a*) (Gobin et al., 2002), were selected from previous published studies. The remaining primers used, were designed in the Primer Blast (National Library of Medicine). Primer characteristics are shown in Table 3.

Table 3 - Primers characteristics

Gene	Primer Sequence (F/R)	$T_{annealing}$ (°C)	Size (bp)
ob	TCTTGTCCCCTCTTGACCCA	52.60	183
	AGCTTGTGTTGCTGGGAGTT		
CPT1A	GCAGCGTTCTTTGTGACGTT	51.86	184
	AGGAGTGTTCAGCGTTGAGG		
SLC1A5	TCTGGCTGGTAACCGCTACT	52.81	107
	GAGTTTCTCTGGGTGGGAGC		
GLS1	TCTACAGGATTGCGAACGTCT	50.31	100
	CTTTGTCTAGCATGACACCATCT		

MPC1	ATTTGCCTACAAGGTACAGCC AGTCATCTCGTGTTTGATAAGCC	50.05	109
SLC2A4	TCCACCAACAACACCGAGAC CGACCAGCATCTTCGAGACA	52.20	117
RPII	CTTCACGGTGCTGGGCATT GTGCGGCTGCTTCCATAA	52.20	239
LDHA	CGACCGCCCGACGTG TAAGGAAAAGGCTGCCATGTTG	52.94	264
FABP4	GTAGGAGTGGGCTTTGCCAC ACGCATTCCACCACCAGTTT	53.01	287
β-actin	CCAACCGCGAGAAGATGA CCAGAGGCGTACAGGGATAG	53.10	97

T – temperature; bp – bases par; F – Forward; R – Reverse

A mixture containing 1 µL cDNA, the specific forward and specific reverse primer (final concentration 0.4 µM), and the NZYTaq II 2× Green Master Mix (MB35801, NZYTech, Lisbon, Portugal), for a total volume of 12.5 µL, was prepared. A negative control was prepared in which the cDNA was replaced by nuclease-free water. The RT - control obtained during the cDNA synthesis was also included in the PCR.

PCR was performed using the following conditions:

Table 4 - Protocol used in Conventional PCR

	$T_{annealing}$ (°C)	**Time**	**N° of cycles**
Ativation	95	5 min	1
Desnaturation	95	30 s	**35 cycles** (*β-actin*, *CPT1a*, *GLS1*, *FABP4*, *LDHA*, *MPC1* and *ob*) **30 cycles** (*RPII*)
Annealing	**56ºC** (*CPT1a*, *GLS1*, *MPC1* and *ob*) **50ºC** (*β-actin*, *FABP4*, *LDHA* and *RPII*): **54ºC** (*SLC1A5* and *SLC2A4*)	30 s	
Extension	72	1 min	
Final Desnaturation	72	7 min	1
Conservation	4	∞	1

After gene amplification, PCR products were analyzed by electrophoresis using a 2% agarose gel (16500- 500, Invitrogen™, Waltham, MA, USA) with 1% Xpert Green DNA Stain (GS01.001, GRiSP, Porto, Portugal). The electrophoresis was performed at 100V and 400 mA for 45 minutes. The molecular weight marker used for electrophoresis was NZYDNA Ladder VI (MB08901, NZYTech, Portugal).

Gel images were acquired using the ChemiDoc™ XRS (Bio-Rad, USA) accoupled with the BioRad ImageLab 6.1 software.

3.2.4 Quantitative Real-Time Polymerase Chain Reaction (qRT-PCR) analysis

Quantification of *ob* (leptin), *CPT1a* (Carnitine Palmitoyl Transferase 1a), *SLC1A5* (Neutral amino acid transporter (e.g., Glutamine transporter), *GLS1* (glutaminase 1), *SLC2A4* (Glucose transporter type 4 – GLUT4), *LDHA* (Lactate dehydrogenase enzyme), *FABP4* (Fatty acid-binding protein 4) and housekeeping genes *β-actin* and *RPII* (RNA polymerase II) expression was achieved by quantitative Real-Time Polymerase Chain reaction (qRT-PCR), following the instructions given by NZYSpeedy qPCR Green Master Mix (2×) (Nyztech). The housekeeping genes were chosen according to previously validated genes for qRT-PCR analysis in human VAT (Mehta et al., 2010).

In each 96-well plate, 0.4 µM of forward and reverse primers, 4.17 ng/µL of cDNA, 8 µL of NZYSpeedy qPCR Green Master Mix (2×) (MB22402, NZYTech, Portugal), and H2Ost (to a total of 16 µL) was added. No cDNA was added in the negative control. A duplicate was performed for each sample. After mix preparation, samples were placed in the CFX Connect™ Real-Time System (Bio-Rad, USA). The three-step cycling qRT-PCR program was performed as described in table 5. The quantitative analysis was followed and obtained through by software CFX-Maestro™ (Bio-Rad).

Table 5 - The three-step cycling qRT-PCR program used

	$T_{annealing}$ (°C)	Time	N° of cycles
Ativation	95	2 min	1
Desnaturation	95	5 s	**35 cycles** (, *CPT1a*, *GLS1*, *MPC1*) **40 cycles** (*β-actin*, *FABP4*, *LDHA*, *ob*, *RPII*)
Annealing	**50°C** (*β-actin*, *FABP4*, *LDHA* and *RPII*) **56°C** (*CPT1a*, *GLS1*, *MPC1*) **60°C** (*ob*)	30 s	
Extension	72	1 min	
Final Desnaturation	72	7 min	1

The analysis of qRT-PCR data was made using the comparative CT method. Individual relative gene expression values were calculated using the following formula:

$$Fold\ Change = 2^{-\Delta C_T} = 2^{-(C_T\ gene\ of\ interest\ -\ C_T\ housekeeping\ gene)}$$ (Schmittgen & Livak, 2008)

SLC2A4 and *SLC1A5* gene expression quantification was ongoing at the time of writing.

3.3 VAT Bioenergetic analysis

3.3.1 Oxygen consumption rate assessment

Agilent Seahorse XF technology evaluates cellular or live tissue energy metabolism. The mitochondrial respiration is evaluated through the measurement of the oxygen consumption rate (OCR) of the cells or tissues, in real time.

In day before the VAT collection, the sensor cartridge was hydrated with a commercial calibration solution (XF Calibrant pH 7.4, Agilent Technologies, Santa Clara, CA, USA), at 37ºC in a CO_2-free incubator. On the following day, VAT fragments (~5 mg) were placed and attached to the bottom of the well by capture screens and incubated in a commercial medium (Seahorse XF DMEM Medium, pH 7.4, 103575 - 100, Agilent Technologies), for at least 45 minutes, at 37°C, in the CO_2-free incubator. After that, VAT was incubated in a seahorse assay medium supplemented with 0.01 mM glucose (103577 - 100, Agilent Technologies), 2 µM glutamine (103579 - 100 Agilent Technologies), 0.17 mM of Sodium Palmitate (P9767 – 5G, Sigma Aldrich, St. Louis, MO, USA) and 0.5 mM of L-Carnitine (C0283- 1G, Sigma Aldrich) and placed in the Seahorse instrument (Seahorse® XFe24 Analyzer, Agilent Technologies). After an initial period of equilibration (52 minutes), metabolic pathway inhibitors and electron transport chain modulators were automatically added to VAT wells in a sequential order. For that, cartridges placed above the incubation plates were filled with different solutions, as represented in Figure 7.

A

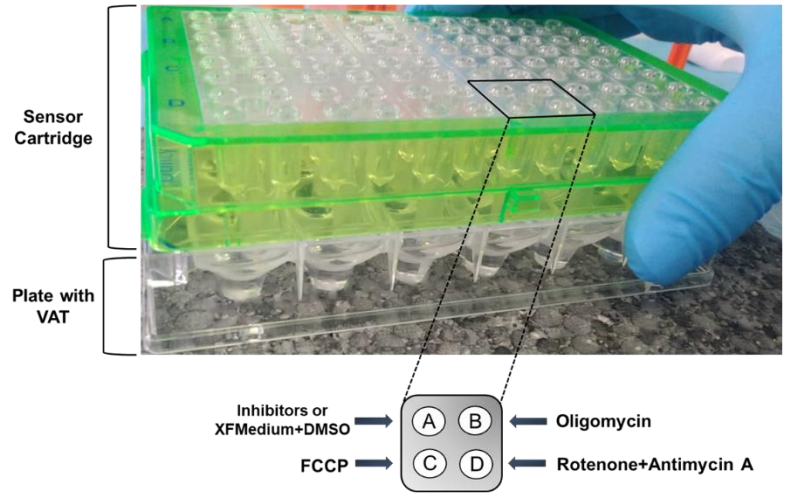

B

Blank	A: Media+DMSO B: Oligomycin C: FCCP D: Rot+ Antimycin A	A: Media+DMSO B: Oligomycin C: FCCP D: Rot + Antimycin A	A: Media+DMSO B: Oligomycin C: FCCP D: Rot + Antimycin A	A: BPTES B: Oligomycin C: FCCP D: Rot + Antimycin A	A: BPTES B: Oligomycin C: FCCP D: Rot + Antimycin A
A: Etomoxir B: Oligomycin C: FCCP D: Rot + Antimycin A	A: Etomoxir B: Oligomycin C: FCCP D: Rot + Antimycin A	A: Etomoxir B: Oligomycin C: FCCP D: Rot + Antimycin A	Blank	A: BPTES B: Oligomycin C: FCCP D: Rot + Antimycin A	A: BPTES+UK5099 B: Oligomycin C: FCCP D: Rot + Antimycin A
A: Eto+UK5099 B: Oligomycin C: FCCP D: Rot + Antimycin A	A: Etomoxir+UK5099 B: Oligomycin C: FCCP D: Rot + Antimycin A	Blank	A: Eto+UK5099 B: Oligomycin C: FCCP D: Rot + Antimycin A	A: BPTES+UK5099 B: Oligomycin C: FCCP D: Rot + Antimycin A	A: BPTES+UK5099 B: Oligomycin C: FCCP D: Rot + Antimycin A
A: UK5099 B: Oligomycin C: FCCP D: Rot + Antimycin A	A: UK5099 B: Oligomycin C: FCCP D: Rot + Antimycin A	A: UK5099 B: Oligomycin C: FCCP D: Rot + Antimycin A	A: Etomoxir+BPTES B: Oligomycin C: FCCP D: Rot + Antimycin A	A: Etomoxir+BPTES B: Oligomycin C: FCCP D: Rot + Antimycin A	A: Etomoxir+BPTES B: Oligomycin C: FCCP D: Rot + Antimycin A

Figure 7 – A) Schematic representation of the incubation plate and sensor cartridges **B)** Plate layout with the solutions placed in the different ports of the cartridge. The 3 gray squares represent empty wells that work as assays' calibrators. (DMSO - Dimethyl Sulfoxide; Rot – Rotenone, FCCP – carbonyl cyanide-p-trifluoromethoxyphenylhydrazone; BPTES - Bis-2-(5-phenylacetamido-1,3,4-thiadiazol-2-yl) ethyl sulfide).

The port **A** of the cartridge (first solution to be added) was filled with different metabolic pathway inhibitors: the mitochondrial pyruvate carrier inhibitor (UK5099) (final concentration of 4 µM (5.04817.0001, EMD Millipore Corporation, USA), the glutaminase inhibitor BPTES, ((Bis-2-(5-phenylacetamido-1,3,4-thiadiazol-2-yl)ethyl sulfide, final concentration of 6 µM, SML0601, Sigma Aldrich) and the inhibitor of carnitine palmitoyltransferase-1, Etomoxir (final concentration of 8 µM, 236020, EMD Millipore Corporation). Those solutions were added singly or in combinations to VAT wells, during the assay (as shown in Figure 8). Medium with dimethyl sulfoxide (DMSO, final concentration of 0.2%, D2650 - 5X10ML, Sigma Aldrich) was used as control. All conditions were performed in triplicate. The ports B, C and D of the cartridge were filled with the following electron transport chain modulators: port **B** - oligomycin solution (final concentration of 12.5 µg/mL, O4876, Sigma Aldrich), an ATP synthase inhibitor; port **C** – FCCP (carbonyl cyanide-p-trifluoromethoxyphenylhydrazone, final

concentration of 8 µM, C2920, Sigma Aldrich), an uncoupler of mitochondrial oxidative phosphorylation and port **D** - combination of Rotenone (final concentration of 2 µM, R8875, Sigma Aldrich) and Antimycin A (final concentration of 4 µM, A8674, Sigma Aldrich), inhibitors of the mitochondrial complexes 1 and 3, respectively.

VAT OCR was evaluated during a total of 6 hours and 40 minutes. Metabolic pathways inhibitors were added to the wells containing VAT 45 minutes after the beginning of the assay; oligomycin after 80 minutes; FCCP after 140 minutes and the rotenone and Antimycin A mixture after 260 minutes. Results were exported to the Seahorse Wave 2.6.3 software, and the data obtained for each condition was later normalized for the amount of protein at each VAT fragment.

All concentrations and timepoints used in this study, were previously optimized by our research group. The main actions of the inhibitors and modulators used in these bioenergetic assays are represented in Figure 8.

A

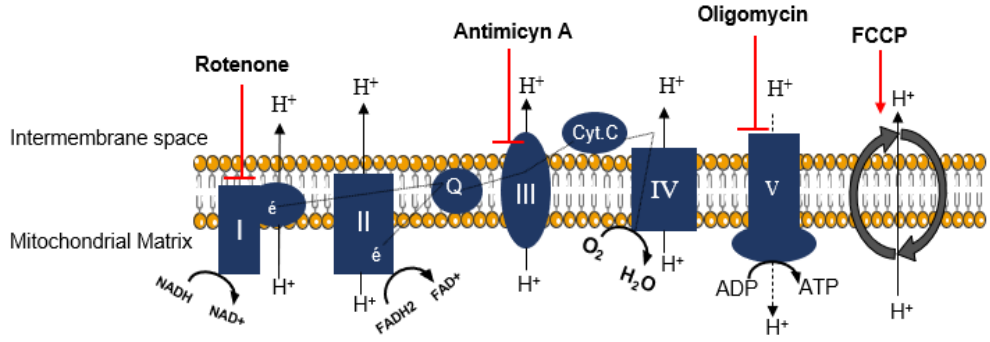

B

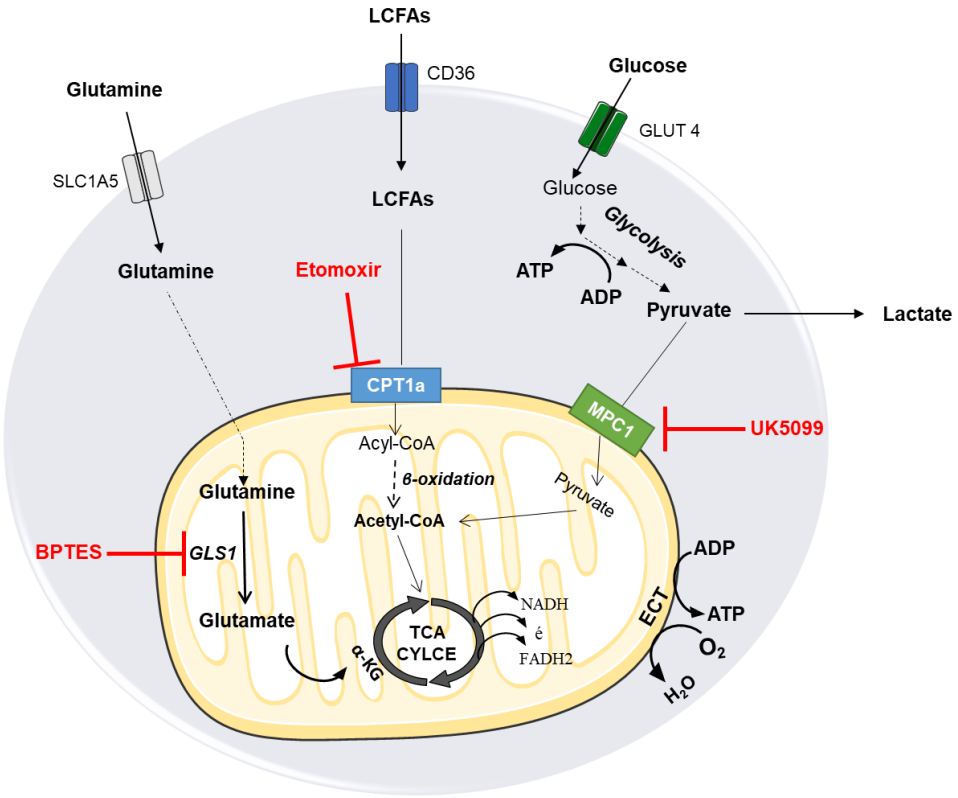

Figure 8 - Summary of the targets and effects of the **(A)** mitochondrial respiration modulators and **(B)** inhibitors of the metabolic pathways used in this study. Adapted from (Agilent, 2020).

3.3.2 Total Protein extraction and quantification

At the end of the bioenergetic assay, VAT fragments were used to extract total proteins using a protocol previously optimized for adipose tissue proteins extraction (Diaz Marin, Crespo-Garcia, Wilson, & Sapieha, 2019). VAT fragments were incubated overnight, at 4ºC in RIPA buffer (RO278 - 500ML, Sigma Aldrich) supplemented with protease (04693124001, Roche, Basel, Switzerland) and phosphatase inhibitors (04906845001, Roche, Basel, Switzerland). After that, VAT fragments were lysed using the FastPrep®-24 Instrument (MP Biomedicals, USA) at a speed of 6.0 m/s for 30s, for at least 3 times with a resting period of 5 minutes, in ice, between the lysis procedures. After lysis, samples were incubated on ice for 1h and then centrifuged at 20000g, for 15 min, at 4ºC. Proteins were quantified using the commercial Pierce™ BCA Protein Assay Kit (23225, Thermo Fisher Scientific, Rockford, USA). Briefly, bovine serum albumin (BSA) standards [0 to 2000 µg/mL] and the working reagent (WR) were prepared, following the kit instructions. In a 96-well plate, 25 µL of each sample or BSA standard and 200 µL of WR reagent were added to each well, in duplicate. The plate was incubated for 30 minutes at 60ºC, in a dark room. Finally, the absorbance (570 nm) was read in the microplate reader (Thermo Scientific™ Multiskan™ FC

Microplate Photometer, Thermo Fisher Scientific). The standard curve with a linear fit algorithm was used to determine protein concentration. The values obtained were used to normalize the OCR results.

3.3.3 Respiratory parameters calculations

From the data obtained during the bioenergetic assays, it was possible to calculate the standard parameters that define the tissue's respiratory signature, as shown in Figure 9.

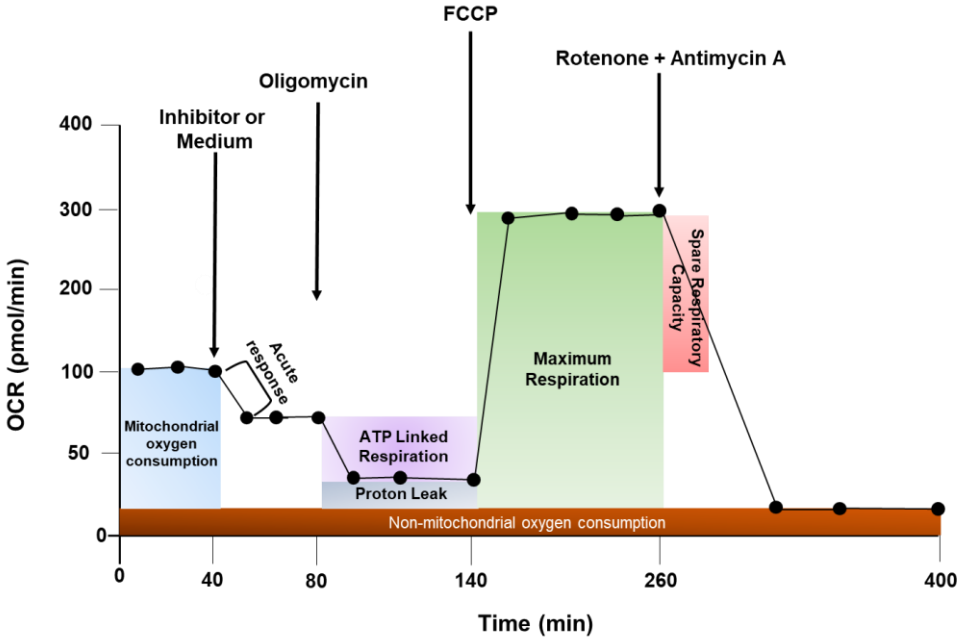

Figure 9 - Schematic representation of a graphic obtained in the Seahorse assays when addition of different metabolic inhibitors and ETC modulators (XF Substrate Oxidation Stress Tests). From these graphs, it is possible to calculate the different parameters of mitochondrial or non-mitochondrial oxygen consumption: Total and Mitochondrial Basal oxygen consumption, ATP linked-respiration, Proton Leak, Maximum respiration, non-mitochondrial oxygen consumption, spare respiratory capacity, and acute response. Figures adapted from (Rose et al., 2014) and (Agilent, 2020).

The respiratory parameters calculated, in this study, are shown in **Table 6.**

Table 6 - Respiration parameters meaning and calculation formulas.

Assay Parameter	***Meaning/ Equation***
Total Basal Oxygen Consumption	Oxygen consumed by the tissue for mitochondrial respiration and other oxygen-dependent processes (e.g., cyclooxygenases, ROS production)
	Last measure before the injection of the metabolic pathways' inhibitor
Non-mitochondrial oxygen consumption	Oxygen consumed after inhibition of the electron transport chain, by other oxygen-dependent processes
	Minimum rate measurement after Rotenone/Antimycin A injection
Mitochondrial Basal Respiration	Oxygen consumed in the electron transport chain, under basal conditions

	(Last rate measurement before any injection) – (Non-Mitochondrial Oxygen Consumption)
ATP Linked Respiration	Oxygen consumed by the mitochondria, for the ATP production, to satisfy the cell's energy needs
	(Last rate measurement before Oligomycin injection) – (Minimum rate measurement after Oligomycin injection)
Maximum Respiration	Maximum rate of respiration that the cell can achieve under a physiological energy demand
	(Maximum rate measurement after FCCP injection) – (Non-Mitochondrial Oxygen Consumption)
Spare Respiratory Capacity	Amount of oxygen consumption not used for basal respiration but that can be used in case of a sudden increase in energy demand
	(Maximum Respiration) – (Basal Respiration)
Acute response	Changes in the basal oxygen consumption rate due to the influence of a substrate oxidation inhibitor
	(Last rate measurement before Oligomycin injection) – (Last rate measurement before acute inhibitor injection)
Proton leak	Oxygen consumption rate due to the escape of protons across the inner mitochondrial membrane. It is independent of the ATP synthesis.
	(Minimum rate measurement after Oligomycin injection) – (Non-Mitochondrial Oxygen Consumption)

3.4 Statistical analysis

The statistical analysis was performed with the GraphPad® Prism software (USA), version 8.0.1 for Windows. Qualitative and Quantitative variables are expressed as percentage (%) and mean ± standard error of the mean, respectively. The normality of the variables was evaluated using the unpaired Student's t-test for variables that followed a normal distribution and the Mann-Whitney test for the variables without a normal distribution. Two or more groups were compared using the Friedman test. The Spearman r test or Pearson test was used to correlate two different variables, depending on the normality distribution. A $p<0.05$ were considered statistically significant.

4 Results

4.1 Subjects' anthropometric characteristics

Anthropometric characteristics of the patients are present in table 7. All patients were female (n=15), with an average age of 44.93 ± 3.17 years (range 23-62 years), an average

weight of 108.1 ± 3.83 kg (range 85-135 kg) and an average BMI of 43.00 ± 6.19 kg/m^2 (ranging from 35.40–54.40 kg/m^2).

Table 7 - Study subject´s Anthropometric

	Total	BMI<40 kg/m^2	BMI ≥40 kg/m^2
N° of patients	15	7	8
Age (years)	44.93 ± 3.17	45.57 ± 4.85	44.38 ± 4.48
Weight (kg)	108.1 ± 3.83	99.00 ± 3.37	117.10 ± 4.99
BMI (kg/m^2)	43.00 ± 1.60	37.53 ± 0.58	47.19 ± 1.52

The values are presented as mean ± standard error of the mean. BMI- body mass index.

4.2 Primers validation

The figure 10 shows the agarose gel pictures where the specificity of the primers used to identify and quantify the expression of the genes *SLC2A4*, *FABP4*, *LDHA*, *β-actin* (Fig.10A), *CPT1a*, *GLS1*, *MPC1* (Fig.10B), *ob* (Fig.10C), *RPII* (Fig.10D) and *SLC1A5* (Fig.10E) was confirmed.

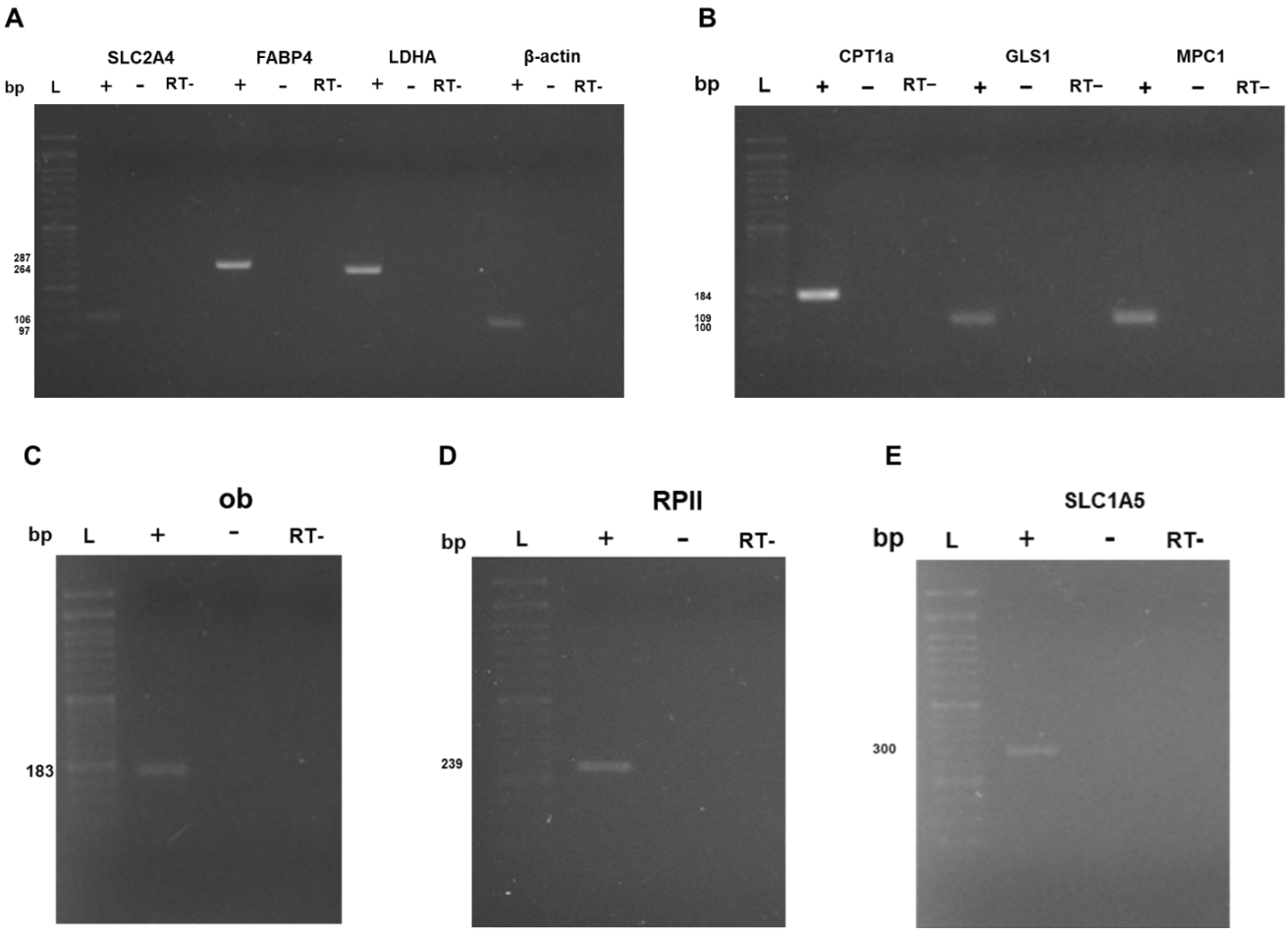

Figure 10 – Identification of A) *SLC2A4*, *FABP4*, *LDHA*, *β-actin genes*; B) *CPT1a*, *GLS1* and *MPC1* genes; C) *ob* gene; D) *RPII gene* and E) *SLC1A5* gene. Agarose gel pictures were taken in the ChemiDoc™ XRS + Image Lab (Bio-Rad). L- NZYDNA Ladder VI; + Positive control; - Negative control; RT− without enzyme transcriptase reverse; *SLC2A4* – GLUT4 (Glucose

transporter type 4), *FABP4* – Fatty Acid Binding-Protein 4; *LDHA* – Lactate Dehydrogenase; *CPT1a* – Carnitine Palmitoyl Transferase 1a; *GLS1* – Glutaminase 1; *MPC1* – Mitochondrial Pyruvate Carrier 1; *ob* - leptin; *RPII* – RNA polymerase; *SLC1A5* - Neutral amino acid transporter.

4.3 Gene expression

The expression of the analyzed genes was not significantly different in the VAT of patients with a BMI≥ 40 kg/m^2 when compared to the VAT of patients with a BMI <40 kg/m^2 (Figure 11).

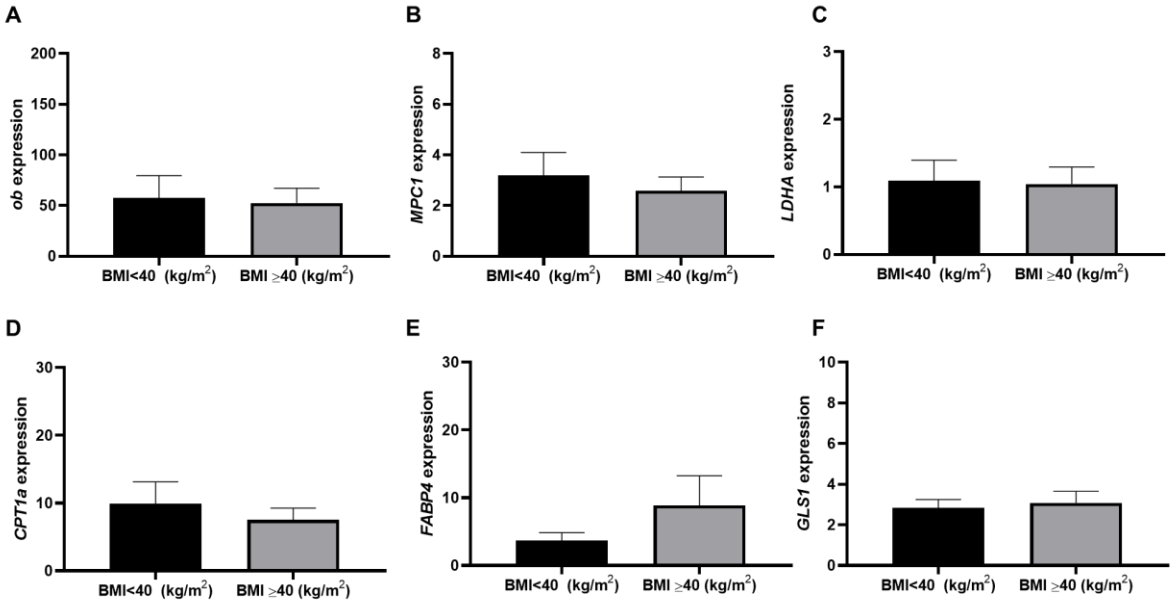

Figure 11 – Expression of A) *ob*; B) *MPC1*; C) *LDHA*; D) *CPT1a*; E) *FABP4* and F) *GLS1* genes in the VAT of patients with a BMI <40 kg/m^2 or a BMI ≥ 40 kg/m^2. ob – Leptin; *MPC1* – Mitochondrial Pyruvate Carrier 1; *LDHA* - Lactate Dehydrogenase A; *CPT1a* – Carnitine Palmitoyl Transferase 1A; *FABP4* - Fatty Acid Binding-Protein 4; *GLS1* – Glutaminase 1; BMI – Body Mass Index. The results were normalized to expression of housekeeping genes (*RPII* and *β-actin*).

4.4 Bioenergetic Assays

4.4.1 Correlation between subjects age and the bioenergetic parameters

We found that the included patients presented a high range of age (23-62 years). So, in order to understand if this factor would influence the VAT metabolism, we performed correlations between age and the different calculated metabolic parameters. No significant correlations were observed between the patients' age and the different VA3T energetic parameters (Table 8).

Table 8 – Correlation between Age (years) and visceral adipose tissue respiration parameters.

Parameter	Correlation (R value)	p value
Total Basal Oxygen Consumption	0.01	ns
Mitochondrial Basal Respiration	0.20	ns
Non-mitochondrial oxygen consumption	0.02	ns

ATP Link Respiration	0.31	ns
Proton Leak	0.28	ns
Maximum Respiration	0.21	ns
Spare Respiratory Capacity	0.13	ns

4.4.2 VAT Respiratory parameters of patients with a BMI <40 and ≥ 40 kg/m^2

Basal respiration, mitochondrial respiration, non-mitochondrial oxygen consumption; maximum respiration; spare respiratory capacity; proton Leak, ATP link respiration and the influence of metabolic pathways inhibitors in VAT were evaluated and compared between patients with a BMI <40 and ≥40 kg/m^2 (severe obesity). Exemplificative graphics, obtained during the bioenergetic assays, are shown in Figure 12.

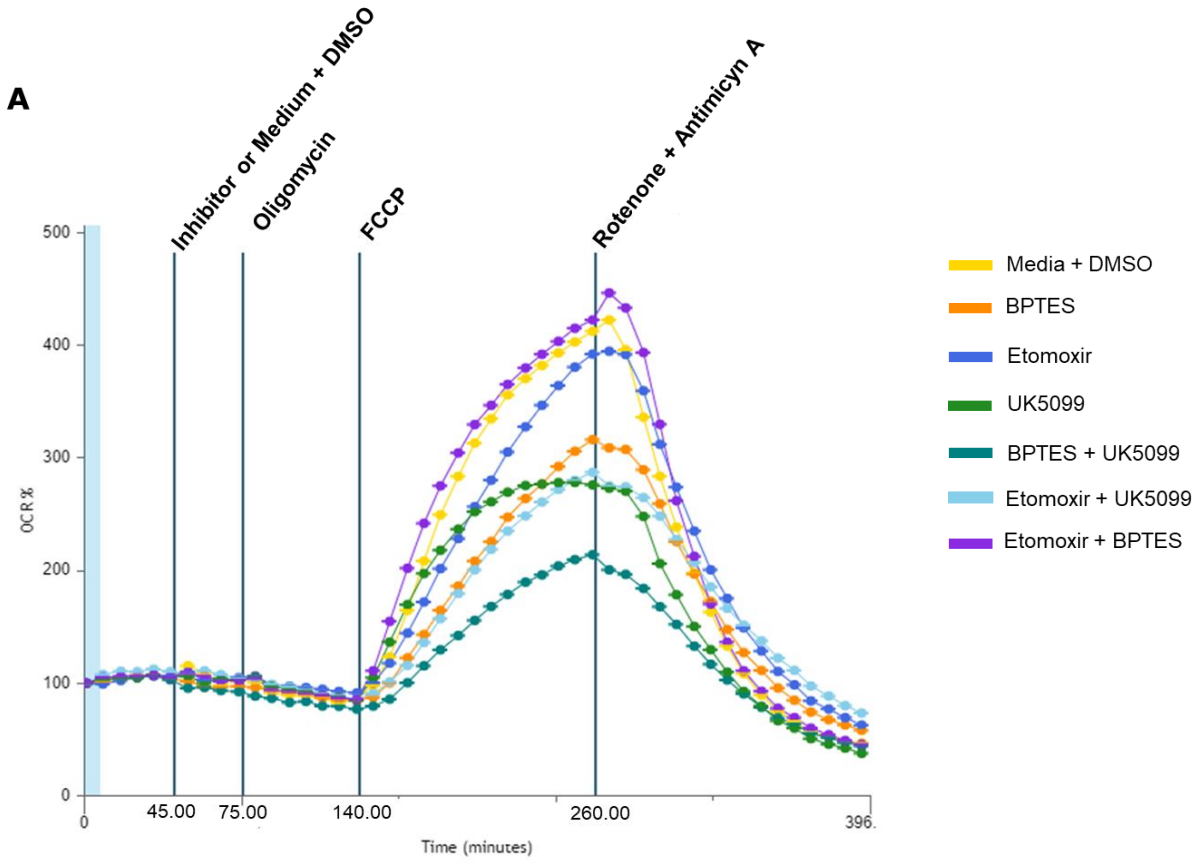

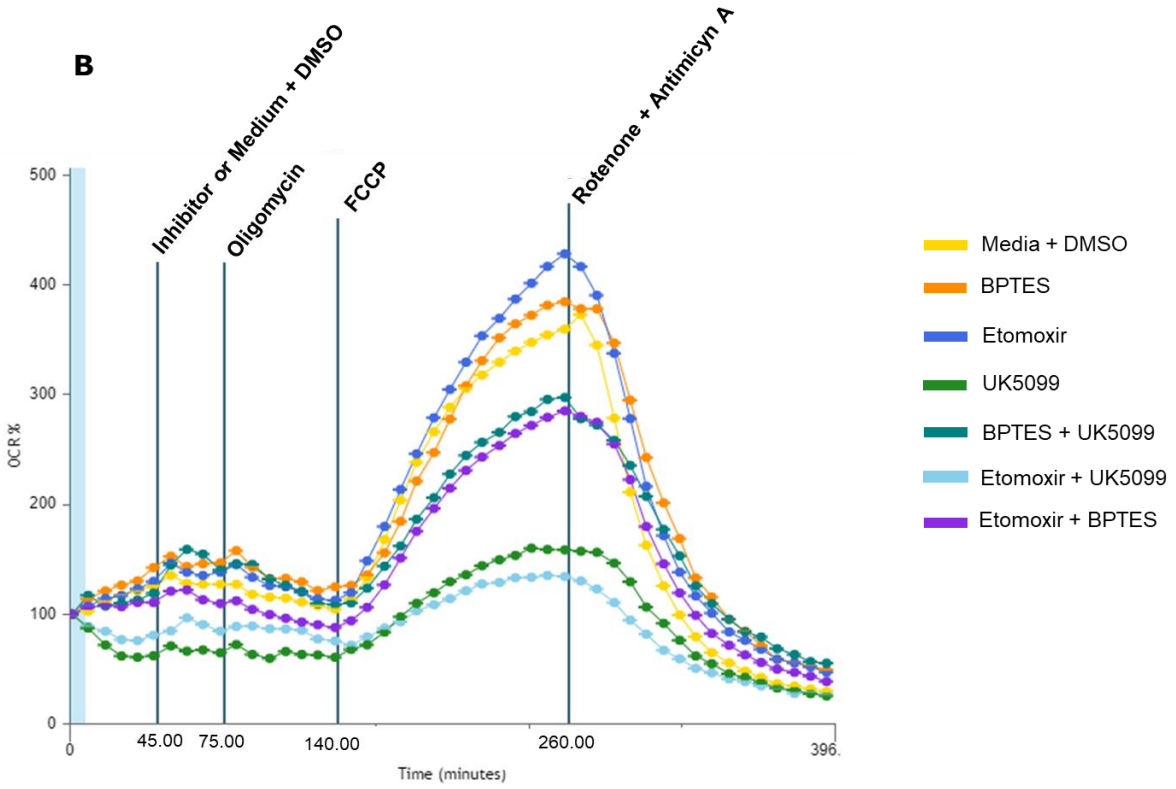

Figure 12 - Oxygen consumption rate (OCR) during the bioenergetic assay in **A)** VAT pertaining to a patient with a BMI <40 kg/m^2 and **B)** VAT pertaining to a patient with a BMI ≥40 kg/m^2. Graphics were obtained by Seahorse Software Wave (Agilent Technologies, USA).

4.4.2.1 Under basal conditions

Under basal conditions (used as assay control), the only difference found in the VAT of patients with BMI ≥40 kg/m^2 when compared with the VAT of patients with BMI <40 kg/m^2 was the non-mitochondrial respiration rate that was higher (0.04 ± 0.01 ρmol/min/μg/mL of total protein vs 0.02 ± 0.002 ρmol/min/μg/mL of total protein, p <0.05). Despite the fact that the total basal oxygen consumption, the mitochondrial basal respiration and the maximum respiration was numerically higher in patients with a BMI ≥40 kg/m^2 (total basal oxygen consumption: 0.10 ± 0.02 ρmol/min/μg/mL; mitochondrial basal respiration: 0.06 ± 0.01 ρmol/min/μg/mL; maximum respiration; 0.27 ± 0.05 ρmol/min/μg/mL), no statistically significant differences were observed (Figure 13).

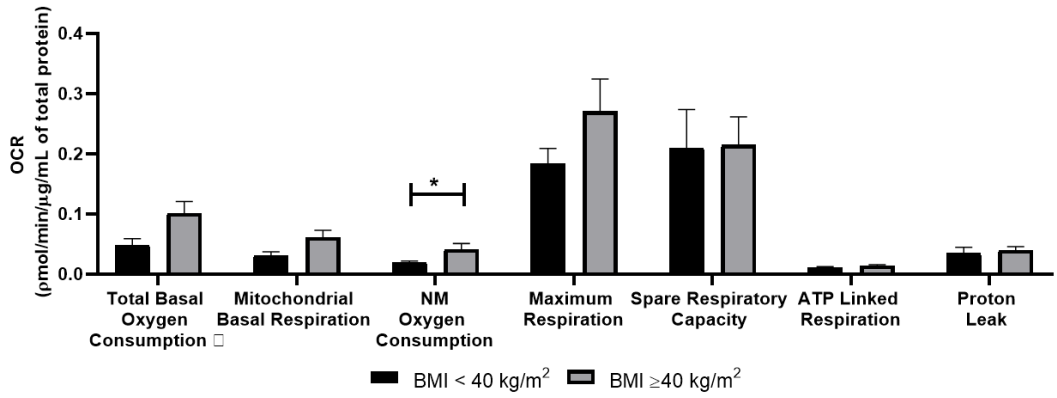

Figure 13 - Respiratory parameters within VAT of patients with a BMI <40 kg/m^2 and BMI ≥40 kg/m^2 (Mann-Whitney test * p<0.05). **OCR** - Oxygen Consumption Rate; **NM** – Non-Mitochondrial.

4.4.2.2 Influence of substrate oxidation pathways inhibitors

Evaluating the VAT profile of all patients with obesity included in this study, the maximum respiration and spare respiratory capacity were significantly lower under the influence of UK5099 and BPTES inhibitors combined when compared with basal conditions (maximum respiration: 58.46 ± 11.53 % vs 100.00 ± 18.94 %, p<0.001; spare respiratory capacity: 49.94 ± 12.56 % vs 100.00 ± 17.56 %, p<0.01) (Fig. 14A and 14B). The VAT ATP link respiration and proton leak were higher under the influence of the UK5099 and Etomoxir inhibitors combined when compared with basal conditions (ATP link respiration: 237.50 ± 48.57 % vs 100.00 ± 21.65 %, p<0.05; proton leak: 243.00 ± 62.61 % vs 100.00 ± 14.24 % p<0.05) (Fig 14C and 14D). No significant differences were observed for the remaining parameters (Supplementary Figure S1).

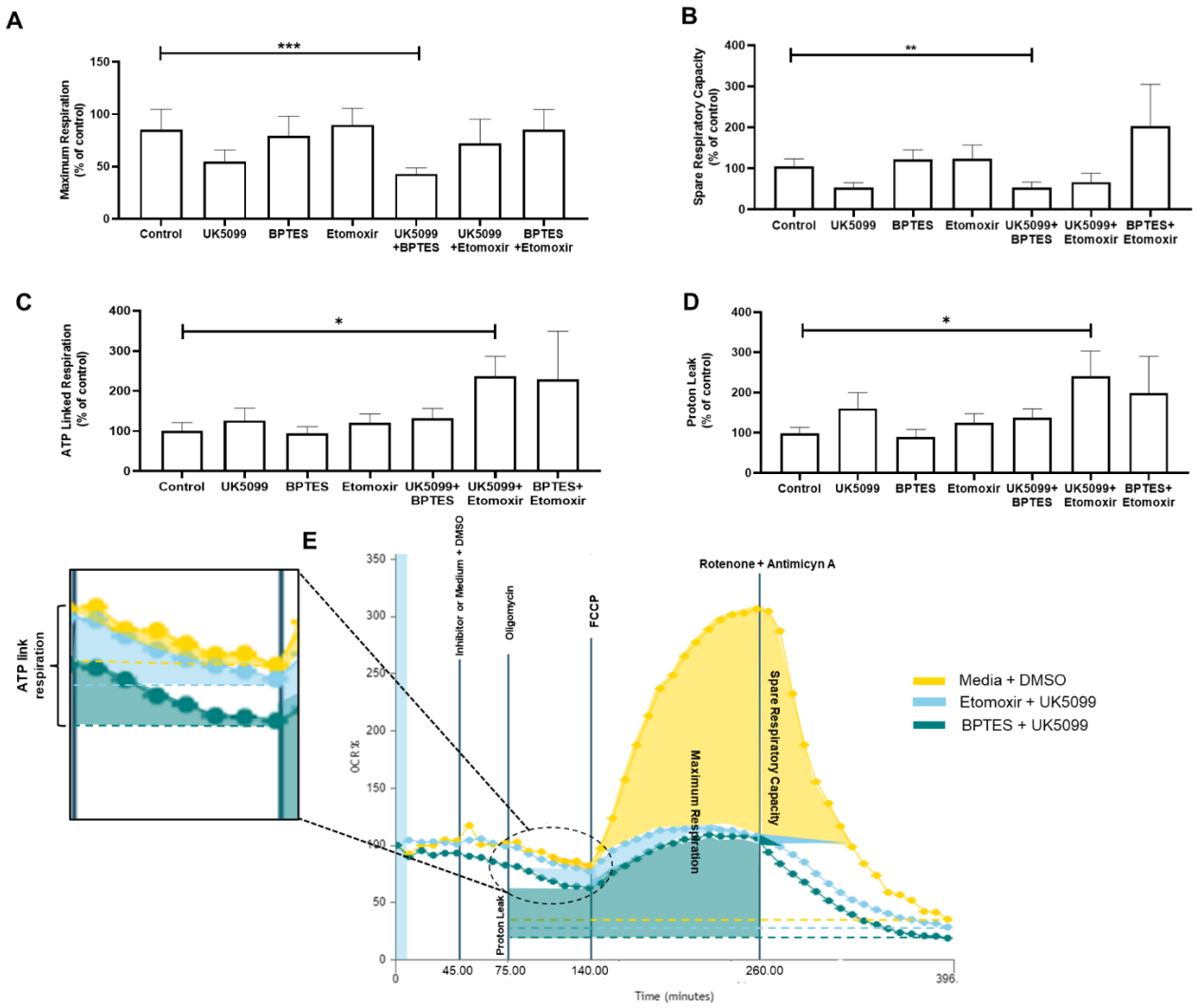

Figure 14 - (A) Maximum Respiration, (B) Spare respiratory capacity, (C) ATP link respiration and D) Proton Leak under the influence of specific inhibitors. Graphic illustrating the OCR of VAT pertaining to patients with obesity (Friedman test * p<0.05, ** p<0.01, *** p<0.001). Graphics OCR vs. Time was obtained in Wave Software (Agilent Technologies).

For patients with a BMI <40 kg/m^2, the VAT maximum respiration and spare respiratory capacity were significantly lower under the influence of the UK5099 and BPTES inhibitors combined when compared to basal conditions (maximum respiration: 43.94 ± 10.49 % vs 100.00 ± 39.57 %, p<0.05; spare respiratory capacity: 49.81± 24.17 % vs 100.00 ± 30.62 %, p<0.05, Fig.15A and C). Contrarily, the proton leak was higher under the influence of UK5099 and Etomoxir inhibitors combined when compared basal conditions (355.50 ± 131.90 % vs 100.00 ± 28.85%, p<0.01, Fig.15E). No other significant differences were observed (Supplementary Figure S2).

For patients with BMI ≥40 kg/m^2, although the maximum respiration and spare respiratory capacity decreased under the influence of UK5099 with BPTES inhibitors combination when compared basal conditions (maximum respiration: 68.17 ± 17.30 % vs. 100.00 ± 20.29 %; spare respiratory capacity: 49.94 ± 12.56 % vs. 100.00 ± 17.56) or

Etomoxir (maximum respiration: 78.79 ± 27.54 % vs. 100.00 ± 20.29 %; spare respiratory capacity: 62.17 ± 20.54 % vs. 100.00 ± 17.56), no statistically significantly differences were observed (Figure 15 and Supplementary Figure S3).

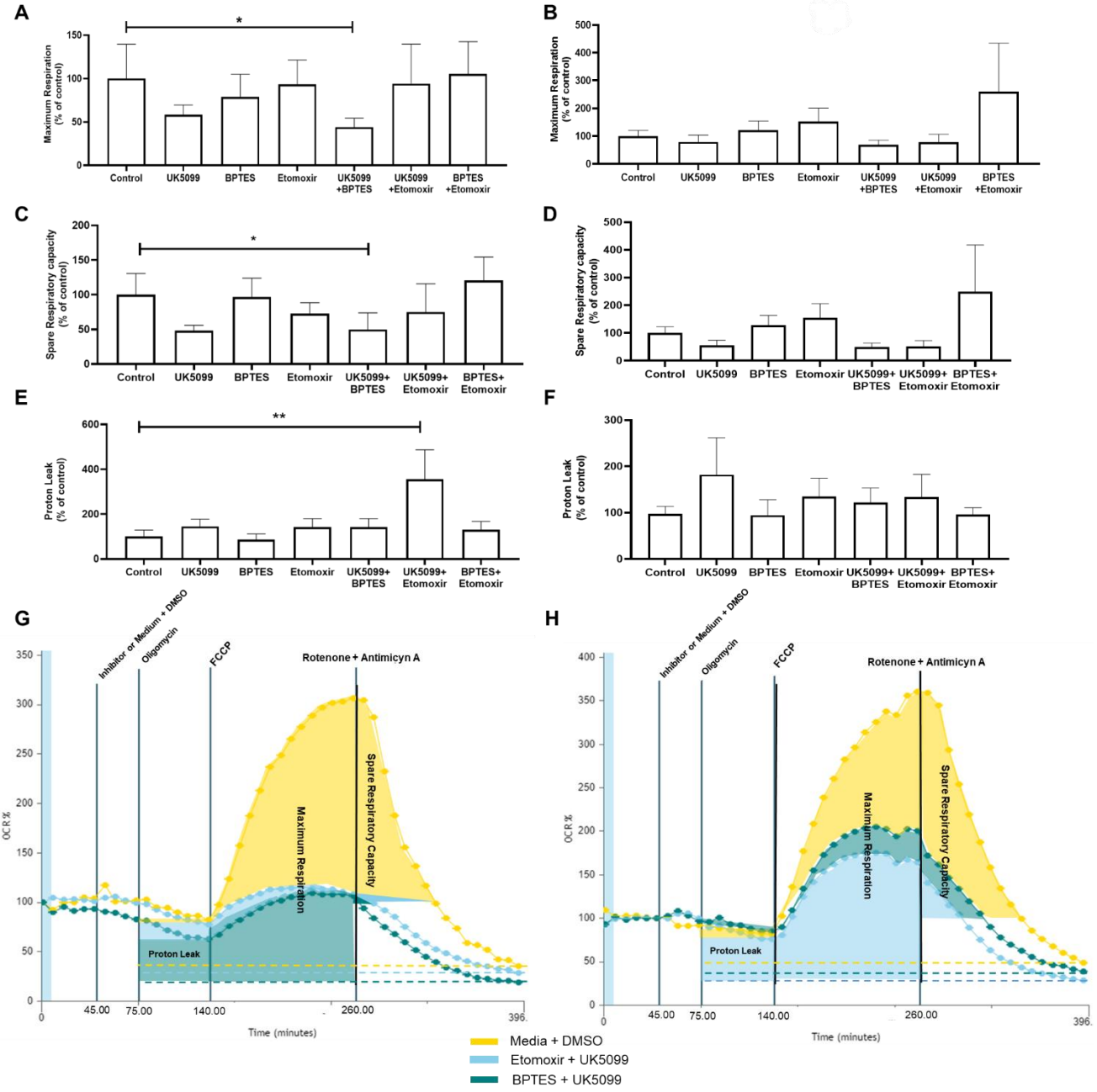

Figure 15 - Influence of the inhibitors in maximum respiration, spare respiratory capacity, and proton leak in VAT of patients with BMI <40 kg/m^2 (A, C and E) and with ≥40 kg/m^2 (B, C, E). (G) and (H): illustrative graphics of the VAT OCR of patients with BMI <40 kg/m^2 and BMI ≥40 kg/m^2 respectively. Graphics OCR vs. Time was obtained in Wave Software (Agilent Technologies). (Friedman test *p<0.05, **p<0.01).

5 Discussion

Bioenergetics corresponds to the energy flow through living systems. Its knowledge is essential for the understanding of pathological mechanisms leading to energy unbalance disorder, to identify biomarkers of disease progression and to identify targets that could lead to new therapeutic strategies. The development of novel bioenergetic analysis equipment's (e.g., extracellular flux analysis, high-resolution respirometry, etc.) enabled a rapid assessment of several metabolic parameters (Chacko et al., 2014; Schmidt, Fisher-Wellman, & Neufer, 2021). Mitochondria are organelles that respond dynamically to changes within its microenvironment and are very susceptible to stress (Chacko et al., 2014). Individuals with obesity were previously described to depict adipose tissue mitochondrial dysfunction (de Mello et al., 2018; Heinonen et al., 2020). However, data on whether mitochondrial dysfunction in the VAT of patients with obesity is similar across different classes of the disease, is still poorly understood. So, the aim of this study was to compare the bioenergetic function and preference in substrate use of VAT pertaining to patients with a BMI < 40 kg/m^2 and a BMI ≥ 40 kg/m^2. For that, VAT harvested during elective surgical procedures was incubated with specific inhibitors of the three main mitochondrial energy substrates: glutamine, pyruvate, and fatty acids; and under the influence of mitochondrial modulators.

Our study found that non-mitochondrial oxygen consumption was higher in the VAT of patients with a BMI ≥ 40 kg/m^2 when compared to those of patients with a BMI < 40 kg/m^2. Obesity is associated with a higher production of ROS and excessive accumulation of pro-inflammatory macrophages in VAT that characterize a chronic low-grade inflammatory state (Graja, Gohlke, & Schulz, 2019). Thus, the greater non-mitochondrial oxygen consumption found in the VAT of patients with BMI ≥ 40 kg/m^2 could result from a higher activity of pro-oxidant and pro-inflammatory enzymes, such as cyclo-oxygenases, cytochrome P450 or NADPH oxidases in response to the increase in VAT inflammation (Chacko et al., 2014).

VAT basal respiration of patients with obesity was not influenced by none of the substrate's inhibitors, supporting previous adipose tissue data showing a high degree of metabolic plasticity (Sakers, De Siqueira, Seale, & Villanueva, 2022). However, under conditions of greater energy demands, in the herein study we demonstrated that pyruvate is the preferential VAT mitochondrial substrate, since the maximum respiration and the percentage of spare capacity decreased when MPC is inhibited and so the entrance of pyruvate to the mitochondria gets blocked. This observation became particularly evident when both pyruvate and glutamine metabolism were inhibited. This is further supported by previous studies which demonstrated that glucose/ pyruvate metabolism inhibition is compensated by the usage of glutamine (Petrus et al., 2020). So, although adipocytes are

reservoirs of fatty acids, those are not used as preferential mitochondrial substrates not even under energy demand or shortage of pyruvate and glutamine.

Under the influence of pyruvate and fatty acid inhibitors, so that only glutamine could be used as mitochondrial energetic substrate, we found an increase in VAT ATP-linked respiration and proton leak. Glutamine is a non-essential amino acid used by adipose tissue to obtain energy through glutaminolysis. This pathway corresponds to the conversion of glutamine into glutamate to produce key metabolic intermediaries for fatty acid biosynthesis and to feed the TCA cycle (Swamy et al., 2016). A previous study found that glutamine was able to reduce glycolysis by inhibiting glucose-6-fostate and 3-fosfoglycerol, which leads to an increase of the TCA cycle activity (Petrus et al., 2020) and to an high rate of NADH and $FADH_2$ generation, used as electron carriers in ETC, and so to higher ATP-linked respiration. Because of increased oxygen consumption by the ETC, there is a greater production of ROS and consequently a rapid depolarization of inner mitochondrial membrane potential ($\Delta\Psi m$). The proton leak is one of the mitochondrial protective mechanisms to decrease ROS production (Fernández-Sánchez et al., 2011; Hue & Taegtmeyer, 2009; Nanayakkara, Wang, & Yang, 2019). Since lipid membranes have a high conductance, it allow protons to migrate across the inner mitochondrial membrane independently of complex V, i.e. proton leak. (Nanayakkara et al., 2019). There are two forms to enable the physiological regulation of proton leakage: basal/constitutive and inducible. In basal/constitutive, proton leakage depends on the fatty acyl composition of the inner phospholipids' membrane. Inducible proton leak depends on specific mitochondrial inner membrane proteins, the uncoupling proteins (UCPs) (Nanayakkara et al., 2019). The UCPs are regulated at the molecular, transcriptional, translational, and proteolytic levels, and several studies suggest, its involvement in cardiovascular disease, oxidative stress, T2D, and immune response (Brookes, 2005; Nanayakkara et al., 2019). UCP-2 is ubiquitously expressed in most cell types and tissues, while UCP-3 is less abundantly expressed (Tian, Ma, Tse, Wong, & Huang, 2018). UCP-1 is the most studied UCP protein, since it was shown to be present in BAT and associated with non-shivering thermogenesis (Monteiro, Freire-Brito, Carrageta, Oliveira, & Alves, 2021). VAT UCP-1, -2 and -3 and UCP-2 expression is lower in individuals with obesity (Kurylowicz et al., 2015; Mahadik, Lele, Saranath, Seth, & Parikh, 2012). A previous study in neuroblastoma cells found that glutamine increases the expression of UCP-2 in the inner mitochondrial membrane (Klotzsch et al., 2015), as a defense mechanism against ROS (Rupprecht, Moldzio, Mödl, & Pohl, 2019). So, we postulate that a similar mechanism may occur in the VAT under the influence of glutamine, since an increase proton leak was observed (Supplementary Figure 4). Previously, glutamine was appointed has having a role in obesity, since glutamine is downregulated in obesity mainly due to the decrease expression

of the glutamine synthetase enzyme (GLUL), leading to inflammation. Glutamine presence seams to attenuate the expression of pro-inflammatory genes/proteins in VAT (Petrus et al., 2020).

Interesting, the decrease in maximum respiration and percentage of spare capacity under the influence of pyruvate and glutamine metabolism inhibitors; and also, the increase of proton leak under the influence of pyruvate and fatty acids metabolism inhibitors seems to be specific characteristics of VAT of patients with a BMI<40 kg/m^2. Although the increase in maximum respiration and percentage of spare capacity under the influence of pyruvate and glutamine metabolism inhibitors also decreased in VAT of patients with severe obesity, no significant differences were observed. Thus, the VAT of this group of patients may have higher metabolic elasticity and under energy demands adapts its metabolism to use the substrate that is available at a given moment. However, in order to understand whether these findings were negatively influenced by small number of subjects in this study, these need to be validated in a larger patient population. Noteworthy, the group in which the significant differences (BMI<40 kg/m^2) were observed, has a smaller number of subjects when compared to the group with a BMI ≥ 40 kg/m^2.

In addition, in the VAT of patients with severe obesity (BMI ≥ 40 kg/m^2), the protective role of glutamine against ROS by increasing proton leak as previously described, does not seem to occur since, when glutamine is the only energetic substrate available, since no differences on the proton leak were observed, contrarily to what was observed for the other group.

The greater inflammatory status previously described in patients with severe obesity (BMI ≥ 40 kg/m^2), may justify this result since inflammation is able to modulate glutamine metabolism (Petrus et al., 2020).

Mitochondrial dysfunction is considered a hallmark of aging (López-Otín, Blasco, Partridge, Serrano, & Kroemer, 2013). Although previous studies found that age leads to a decrease in complex IV activity of ETC (Soro-Arnaiz et al., 2016), in our study, age did not have a significant impact on oxygen consumption or different bioenergetic parameters. This may be because obesity is already associated with considerable mitochondrial dysfunction so that the impact of age is not significant.

In this study, we used VAT instead of isolated adipocytes to better mimic the *in vivo* state. Moreover, *ob* gene expression was used as an indirect measurement of the number of adipocytes in each sample, as this is a gene that is almost solely expressed in the adipocyte. And we found that *ob* gene expression was similar in both groups. In addition, during the bioenergetic assays specific proteins involved in pyruvate, glutamine and fatty

acids metabolism were blocked. Since some of the genes involved in metabolism were already known to be decreased in the VAT of individuals with obesity, such as LDHA (Lopez et al., 2004), CPT1 (Krishnan et al., 2012), GLUT4 (Carvalho, Kotani, Peroni, & Kahn, 2005) and MCP1 (Mardinoglu et al., 2014), we decided to analyze the expression of those genes in both groups. We have demonstrated that all genes analyzed were similarly expressed in the VAT of subjects with a BMI < or ≥ 40 kg/m^2. And so, the bioenergetic results obtained were not influenced by a different expression of these genes in both groups.

In the future, our aim will be to increase the number of patients enrolled in both groups in order to validate the results so far obtained. In addition, patients with different glycemic profiles will be studied since a considerable proportion of patients with obesity also present disglycemia, including pre-T2D and T2D. The expression of other genes related with VAT mitochondrial dysfunction, such as the expression of some Krebs cycle enzymes (e.g., citrate synthase) will also be quantified in our samples. Furthermore, to better understand the mechanism of glutamine action in the VAT of patients with the different BMIs, UCPs expression, GLUT expression, and the activity of antioxidant enzymes as well as the intracellular ROS and ATP levels should be quantified.

6 Conclusion

VAT of patients with severe obesity (BMI ≥ 40 kg/m^2) present a higher non-mitochondrial respiration when compared to VAT of patients with a BMI <40 kg/m^2. Pyruvate seems to be the preferential mitochondrial substrate within the VAT of patients with obesity. However, VAT of patients with a BMI <40 kg/m^2 seems to have a greater sensitivity of the availability of pyruvate and glutamine. Thus, strategies towards modulating substrate availability, as a tool for the treatment for obesity seems to be more likely to be effective in patients with a BMI <40 kg/m^2. Glutamine seems to have a protective role against the ROS production in VAT of patients with a BMI <40 kg/m^2, by increasing the proton leak. This mechanism seems to be dysregulated in VAT of patients with more severe obesity.

7 References

Adams, T. D., Davidson, L. E., Litwin, S. E., Kim, J., Kolotkin, R. L., Nanjee, M. N., . . . Hunt, S. C. (2017). Weight and Metabolic Outcomes 12 Years after Gastric Bypass. *N Engl J Med, 377*(12), 1143-1155. doi:10.1056/NEJMoa1700459

Afshin, A., Forouzanfar, M. H., Reitsma, M. B., Sur, P., Estep, K., Lee, A., . . . Murray, C. J. L. (2017). Health Effects of Overweight and Obesity in 195 Countries over 25 Years. *N Engl J Med, 377*(1), 13-27. doi:10.1056/NEJMoa1614362

Agilent. (2020). Agilent XF Substrate Oxidation Stress Test Kits User Manual. Retrieved from https://www.agilent.com/cs/library/usermanuals/public/user-manual-substrate-oxidation-stress-test-kits-cell-analysis-5994-1164en-agilent.pd

Armstrong, J. S., Whiteman, M., Yang, H., & Jones, D. P. (2004). The redox regulation of intermediary metabolism by a superoxide-aconitase rheostat. *Bioessays, 26*(8), 894-900. doi:10.1002/bies.20071

Berg, L. S. J. L. T. J. M. (2012). *BIOQUÍMICA* (G. K. LTDA. Ed.).

Betz, M. J., & Enerbäck, S. (2018). Targeting thermogenesis in brown fat and muscle to treat obesity and metabolic disease. *Nat Rev Endocrinol, 14*(2), 77-87. doi:10.1038/nrendo.2017.132

Blüher, M. (2019). Obesity: global epidemiology and pathogenesis. *Nature Reviews Endocrinology, 15*(5), 288-298. doi:10.1038/s41574-019-0176-8

Boudina, S., & Graham, T. E. (2014). Mitochondrial function/dysfunction in white adipose tissue. *Exp Physiol, 99*(9), 1168-1178. doi:10.1113/expphysiol.2014.081414

Bournat, J. C., & Brown, C. W. (2010). Mitochondrial dysfunction in obesity. *Curr Opin Endocrinol Diabetes Obes, 17*(5), 446-452. doi:10.1097/MED.0b013e32833c3026

Brookes, P. S. (2005). Mitochondrial H(+) leak and ROS generation: an odd couple. *Free Radic Biol Med, 38*(1), 12-23. doi:10.1016/j.freeradbiomed.2004.10.016

Carvalho, E., Kotani, K., Peroni, O. D., & Kahn, B. B. (2005). Adipose-specific overexpression of GLUT4 reverses insulin resistance and diabetes in mice lacking GLUT4 selectively in muscle. *American Journal of Physiology-Endocrinology and Metabolism, 289*(4), E551-E561. doi:10.1152/ajpendo.00116.2005

Chacko, B. K., Kramer, P. A., Ravi, S., Benavides, G. A., Mitchell, T., Dranka, B. P., . . . Darley-Usmar, V. M. (2014). The Bioenergetic Health Index: a new concept in mitochondrial translational research. *Clin Sci (Lond), 127*(6), 367-373. doi:10.1042/cs20140101

Choe, S. S., Huh, J. Y., Hwang, I. J., Kim, J. I., & Kim, J. B. (2016). Adipose Tissue Remodeling: Its Role in Energy Metabolism and Metabolic Disorders. *Front Endocrinol (Lausanne), 7*, 30. doi:10.3389/fendo.2016.00030

Chondronikola, M. (2020). The role of brown adipose tissue and the thermogenic adipocytes in glucose metabolism: recent advances and open questions. *Current Opinion in Clinical Nutrition & Metabolic Care, 23*(4), 282-287. doi:10.1097/mco.0000000000000662

Coelho, M., Oliveira, T., & Fernandes, R. (2013). Biochemistry of adipose tissue: an endocrine organ. *Arch Med Sci, 9*(2), 191-200. doi:10.5114/aoms.2013.33181

David L. Nelson, M. M. C. (2014). *Princípios de bioquímica de Lehninger* (A. E. LTDA. Ed. 6. ed. ed.).

de Mello, A. H., Costa, A. B., Engel, J. D. G., & Rezin, G. T. (2018). Mitochondrial dysfunction in obesity. *Life Sciences, 192*, 26-32. doi:https://doi.org/10.1016/j.lfs.2017.11.019

Diaz Marin, R., Crespo-Garcia, S., Wilson, A. M., & Sapieha, P. (2019). RELi protocol: Optimization for protein extraction from white, brown and beige adipose tissues. *MethodsX, 6*, 918-928. doi:https://doi.org/10.1016/j.mex.2019.04.010

Engin, A. (2017). The Definition and Prevalence of Obesity and Metabolic Syndrome. *Adv Exp Med Biol, 960*, 1-17. doi:10.1007/978-3-319-48382-5_1

Fenzl, A., & Kiefer, F. W. (2014). Brown adipose tissue and thermogenesis. *Hormone Molecular Biology and Clinical Investigation, 19*(1), 25-37. doi:doi:10.1515/hmbci-2014-0022

Fernández-Sánchez, A., Madrigal-Santillán, E., Bautista, M., Esquivel-Soto, J., Morales-González, A., Esquivel-Chirino, C., . . . Morales-González, J. A. (2011). Inflammation, oxidative stress, and obesity. *International journal of molecular sciences, 12*(5), 3117-3132. doi:10.3390/ijms12053117

Frigolet, M. E., & Gutiérrez-Aguilar, R. (2020). The colors of adipose tissue. *Gac Med Mex, 156*(2), 142-149. doi:10.24875/gmm.M20000356

Gardner, P. R., Raineri, I., Epstein, L. B., & White, C. W. (1995). Superoxide radical and iron modulate aconitase activity in mammalian cells. *J Biol Chem, 270*(22), 13399-13405. doi:10.1074/jbc.270.22.13399

Gobin, S., Bonnefont, J. P., Prip-Buus, C., Mugnier, C., Ferrec, M., Demaugre, F., . . . Thuillier, L. (2002). Organization of the human liver carnitine palmitoyltransferase 1 gene (CPT1A) and identification of novel mutations in hypoketotic hypoglycaemia. *Hum Genet, 111*(2), 179-189. doi:10.1007/s00439-002-0752-0

Graja, A., Gohlke, S., & Schulz, T. J. (2019). Aging of Brown and Beige/Brite Adipose Tissue. *Handb Exp Pharmacol, 251*, 55-72. doi:10.1007/164_2018_151

Hauck, A. K., Zhou, T., Hahn, W., Petegrosso, R., Kuang, R., Chen, Y., & Bernlohr, D. A. (2018). Obesity-induced protein carbonylation in murine adipose tissue regulates the DNA-binding domain of nuclear zinc finger proteins. *J Biol Chem, 293*(35), 13464-13476. doi:10.1074/jbc.RA118.003469

Hausladen, A., & Fridovich, I. (1994). Superoxide and peroxynitrite inactivate aconitases, but nitric oxide does not. *The Journal of biological chemistry, 269*, 29405-29408. doi:10.1016/S0021-9258(18)43893-8

Heinonen, S., Jokinen, R., Rissanen, A., & Pietiläinen, K. H. (2020). White adipose tissue mitochondrial metabolism in health and in obesity. *Obesity Reviews, 21*(2), e12958. doi:https://doi.org/10.1111/obr.12958

Hepler, C., & Gupta, R. K. (2017). The expanding problem of adipose depot remodeling and postnatal adipocyte progenitor recruitment. *Molecular and Cellular Endocrinology, 445*, 95-108. doi:https://doi.org/10.1016/j.mce.2016.10.011

Hernández-Aguilera, A., Rull, A., Rodríguez-Gallego, E., Riera-Borrull, M., Luciano-Mateo, F., Camps, J., . . . Joven, J. (2013). Mitochondrial dysfunction: a basic mechanism in inflammation-related non-communicable diseases and therapeutic opportunities. *Mediators Inflamm, 2013*, 135698. doi:10.1155/2013/135698

Hue, L., & Taegtmeyer, H. (2009). The Randle cycle revisited: a new head for an old hat. *American Journal of Physiology-Endocrinology and Metabolism, 297*(3), E578-E591. doi:10.1152/ajpendo.00093.2009

Hurd, T. R., Collins, Y., Abakumova, I., Chouchani, E. T., Baranowski, B., Fearnley, I. M., . . . James, A. M. (2012). Inactivation of pyruvate dehydrogenase kinase 2 by mitochondrial reactive oxygen species. *J Biol Chem, 287*(42), 35153-35160. doi:10.1074/jbc.M112.400002

Ikeda, K., Maretich, P., & Kajimura, S. (2018). The Common and Distinct Features of Brown and Beige Adipocytes. *Trends Endocrinol Metab, 29*(3), 191-200. doi:10.1016/j.tem.2018.01.001

Jang, H., Kim, M., Lee, S., Kim, J., Woo, D.-C., Kim, K. W., . . . Lee, I. (2016). Adipose tissue hyperplasia with enhanced adipocyte-derived stem cell activity in Tc1(C8orf4)-deleted mice. *Scientific Reports, 6*(1), 35884. doi:10.1038/srep35884

Khanna, D., Khanna, S., Khanna, P., Kahar, P., & Patel, B. M. (2022). Obesity: A Chronic Low-Grade Inflammation and Its Markers. *Cureus, 14*(2), e22711-e22711. doi:10.7759/cureus.22711

Kim, J.-w., Tang, Q.-Q., Li, X., & Lane, M. D. (2007). Effect of phosphorylation and S–S bond-induced dimerization on DNA binding and transcriptional activation

by C/EBP&#x3b2. *Proceedings of the National Academy of Sciences, 104*(6), 1800-1804. doi:doi:10.1073/pnas.0611137104

Klotzsch, E., Smorodchenko, A., Löfler, L., Moldzio, R., Parkinson, E., Schütz, G. J., & Pohl, E. E. (2015). Superresolution microscopy reveals spatial separation of UCP4 and F₀F₁-ATP synthase in neuronal mitochondria. *Proceedings of the National Academy of Sciences, 112*(1), 130-135. doi:doi:10.1073/pnas.1415261112

Kowaltowski, A. J., & Vercesi, A. E. (1999). Mitochondrial damage induced by conditions of oxidative stress. *Free Radic Biol Med, 26*(3-4), 463-471. doi:10.1016/s0891-5849(98)00216-0

Krishnan, J., Danzer, C., Simka, T., Ukropec, J., Walter, K. M., Kumpf, S., . . . Krek, W. (2012). Dietary obesity-associated Hif1α activation in adipocytes restricts fatty acid oxidation and energy expenditure via suppression of the Sirt2-NAD+ system. *Genes & development, 26*(3), 259-270. doi:10.1101/gad.180406.111

Kurylowicz, A., Jonas, M., Lisik, W., Jonas, M., Wicik, Z. A., Wierzbicki, Z., . . . Puzianowska-Kuznicka, M. (2015). Obesity is associated with a decrease in expression but not with the hypermethylation of thermogenesis-related genes in adipose tissues. *J Transl Med, 13*, 31. doi:10.1186/s12967-015-0395-2

Kusminski, C. M., & Scherer, P. E. (2012). Mitochondrial dysfunction in white adipose tissue. *Trends Endocrinol Metab, 23*(9), 435-443. doi:10.1016/j.tem.2012.06.004

Kwak, S. H., Park, K. S., Lee, K.-U., & Lee, H. K. (2010). Mitochondrial metabolism and diabetes. *Journal of Diabetes Investigation, 1*(5), 161-169. doi:https://doi.org/10.1111/j.2040-1124.2010.00047.x

Lee, H., Lee, Y. J., Choi, H., Ko, E. H., & Kim, J. W. (2009). Reactive oxygen species facilitate adipocyte differentiation by accelerating mitotic clonal expansion. *J Biol Chem, 284*(16), 10601-10609. doi:10.1074/jbc.M808742200

Liu, Y. M., Lacorte, J. M., Viguerie, N., Poitou, C., Pelloux, V., Guy-Grand, B., . . . Clément, K. (2003). Adiponectin gene expression in subcutaneous adipose tissue of obese women in response to short-term very low calorie diet and refeeding. *J Clin Endocrinol Metab, 88*(12), 5881-5886. doi:10.1210/jc.2003-030886

López-Otín, C., Blasco, M. A., Partridge, L., Serrano, M., & Kroemer, G. (2013). The hallmarks of aging. *Cell, 153*(6), 1194-1217. doi:10.1016/j.cell.2013.05.039

Lu, R. H., Ji, H., Chang, Z. G., Su, S. S., & Yang, G. S. (2010). Mitochondrial development and the influence of its dysfunction during rat adipocyte differentiation. *Mol Biol Rep, 37*(5), 2173-2182. doi:10.1007/s11033-009-9695-z

Lushchak, O. V., Piroddi, M., Galli, F., & Lushchak, V. I. (2014). Aconitase post-translational modification as a key in linkage between Krebs cycle, iron homeostasis, redox signaling, and metabolism of reactive oxygen species. *Redox Rep, 19*(1), 8-15. doi:10.1179/1351000213y.0000000073

Mahadik, S. R., Lele, R. D., Saranath, D., Seth, A., & Parikh, V. (2012). Uncoupling protein-2 (UCP2) gene expression in subcutaneous and omental adipose tissue of Asian Indians: Relationship to adiponectin and parameters of metabolic syndrome. *Adipocyte, 1*(2), 101-107. doi:10.4161/adip.19671

Mancini, M. C., & de Melo, M. E. (2017). The burden of obesity in the current world and the new treatments available: focus on liraglutide 3.0 mg. *Diabetology & Metabolic Syndrome, 9*(1), 44. doi:10.1186/s13098-017-0242-0

Mardinoglu, A., Kampf, C., Asplund, A., Fagerberg, L., Hallström, B. M., Edlund, K., . . . Nielsen, J. (2014). Defining the Human Adipose Tissue Proteome To Reveal Metabolic Alterations in Obesity. *Journal of Proteome Research, 13*(11), 5106-5119. doi:10.1021/pr500586e

Masschelin, P. M., Cox, A. R., Chernis, N., & Hartig, S. M. (2020). The Impact of Oxidative Stress on Adipose Tissue Energy Balance. *Frontiers in Physiology, 10*. doi:10.3389/fphys.2019.01638

Mehta, R., Birerdinc, A., Hossain, N., Afendy, A., Chandhoke, V., Younossi, Z., & Baranova, A. (2010). Validation of endogenous reference genes for qRT-PCR analysis of human visceral adipose samples. *BMC Molecular Biology, 11*(1), 39. doi:10.1186/1471-2199-11-39

Monteiro, B. S., Freire-Brito, L., Carrageta, D. F., Oliveira, P. F., & Alves, M. G. (2021). Mitochondrial Uncoupling Proteins (UCPs) as Key Modulators of ROS Homeostasis: A Crosstalk between Diabesity and Male Infertility? *Antioxidants, 10*(11), 1746. Retrieved from https://www.mdpi.com/2076-3921/10/11/1746

Muñoz, A., & Costa, M. (2013). Nutritionally mediated oxidative stress and inflammation. *Oxid Med Cell Longev, 2013*, 610950. doi:10.1155/2013/610950

Nanayakkara, G. K., Wang, H., & Yang, X. (2019). Proton leak regulates mitochondrial reactive oxygen species generation in endothelial cell activation and inflammation - A novel concept. *Archives of Biochemistry and Biophysics, 662*, 68-74. doi:https://doi.org/10.1016/j.abb.2018.12.002

O'Rourke, R. W., White, A. E., Metcalf, M. D., Olivas, A. S., Mitra, P., Larison, W. G., . . . Marks, D. L. (2011). Hypoxia-induced inflammatory cytokine secretion in human adipose tissue stromovascular cells. *Diabetologia, 54*(6), 1480-1490. doi:10.1007/s00125-011-2103-y

Oshio, L. T., Andreazzi, A. E., Lopes, J. F., Sá, J. P., Bolotari, M., Costa, V. M. G., . . . Peters, V. M. (2020). A paternal hypercaloric diet affects the metabolism and fertility of F1 and F2 Wistar rat generations. *J Dev Orig Health Dis, 11*(6), 653-663. doi:10.1017/s2040174419000904

Petrus, P., Lecoutre, S., Dollet, L., Wiel, C., Sulen, A., Gao, H., . . . Rydén, M. (2020). Glutamine Links Obesity to Inflammation in Human White Adipose Tissue. *Cell Metabolism, 31*(2), 375-390.e311. doi:https://doi.org/10.1016/j.cmet.2019.11.019

Piché, M. E., Tchernof, A., & Després, J. P. (2020). Obesity Phenotypes, Diabetes, and Cardiovascular Diseases. *Circ Res, 126*(11), 1477-1500. doi:10.1161/circresaha.120.316101

Pilkington, A.-C., Paz, H. A., & Wankhade, U. D. (2021). Beige Adipose Tissue Identification and Marker Specificity-Overview. *Frontiers in Endocrinology, 12*, 599134-599134. doi:10.3389/fendo.2021.599134

Rogge, M. M. (2009). The role of impaired mitochondrial lipid oxidation in obesity. *Biol Res Nurs, 10*(4), 356-373. doi:10.1177/1099800408329408

Rose, S., Frye, R. E., Slattery, J., Wynne, R., Tippett, M., Pavliv, O., . . . James, S. J. (2014). Oxidative Stress Induces Mitochondrial Dysfunction in a Subset of Autism Lymphoblastoid Cell Lines in a Well-Matched Case Control Cohort. *PLOS ONE, 9*(1), e85436. doi:10.1371/journal.pone.0085436

Rupprecht, A., Moldzio, R., Mödl, B., & Pohl, E. E. (2019). Glutamine regulates mitochondrial uncoupling protein 2 to promote glutaminolysis in neuroblastoma cells. *Biochim Biophys Acta Bioenerg, 1860*(5), 391-401. doi:10.1016/j.bbabio.2019.03.006

Sakers, A., De Siqueira, M. K., Seale, P., & Villanueva, C. J. (2022). Adipose-tissue plasticity in health and disease. *Cell, 185*(3), 419-446. doi:10.1016/j.cell.2021.12.016

Scandroglio, F., Tórtora, V., Radi, R., & Castro, L. (2014). Metabolic control analysis of mitochondrial aconitase: influence over respiration and mitochondrial superoxide and hydrogen peroxide production. *Free Radic Res, 48*(6), 684-693. doi:10.3109/10715762.2014.900175

Scheja, L., & Heeren, J. (2019). The endocrine function of adipose tissues in health and cardiometabolic disease. *Nature Reviews Endocrinology, 15*(9), 507-524. doi:10.1038/s41574-019-0230-6

Schmidt, C. A., Fisher-Wellman, K. H., & Neufer, P. D. (2021). From OCR and ECAR to energy: Perspectives on the design and interpretation of bioenergetics studies. *Journal of Biological Chemistry, 297*(4), 101140. doi:https://doi.org/10.1016/j.jbc.2021.101140

Schmittgen, T. D., & Livak, K. J. (2008). Analyzing real-time PCR data by the comparative C(T) method. *Nat Protoc, 3*(6), 1101-1108. doi:10.1038/nprot.2008.73

Sharma, A. M., & Padwal, R. (2010). Obesity is a sign - over-eating is a symptom: an aetiological framework for the assessment and management of obesity. *Obesity reviews : an official journal of the International Association for the Study of Obesity, 11*(5), 362-370. doi:10.1111/j.1467-789X.2009.00689.x

Soro-Arnaiz, I., Li, Q. O. Y., Torres-Capelli, M., Meléndez-Rodríguez, F., Veiga, S., Veys, K., . . . Aragonés, J. (2016). Role of Mitochondrial Complex IV in Age-Dependent Obesity. *Cell Rep, 16*(11), 2991-3002. doi:10.1016/j.celrep.2016.08.041

Suchacki, K. J., Tavares, A. A. S., Mattiucci, D., Scheller, E. L., Papanastasiou, G., Gray, C., . . . Cawthorn, W. P. (2020). Bone marrow adipose tissue is a unique adipose subtype with distinct roles in glucose homeostasis. *Nature Communications, 11*(1), 3097. doi:10.1038/s41467-020-16878-2

Swamy, M., Pathak, S., Grzes, K. M., Damerow, S., Sinclair, L. V., van Aalten, D. M. F., & Cantrell, D. A. (2016). Glucose and glutamine fuel protein O-GlcNAcylation to control T cell self-renewal and malignancy. *Nature Immunology, 17*(6), 712-720. doi:10.1038/ni.3439

Tchernof, A., & Després, J. P. (2013). Pathophysiology of human visceral obesity: an update. *Physiol Rev, 93*(1), 359-404. doi:10.1152/physrev.00033.2011

Tian, X. Y., Ma, S., Tse, G., Wong, W. T., & Huang, Y. (2018). Uncoupling Protein 2 in Cardiovascular Health and Disease. *Front Physiol, 9*, 1060. doi:10.3389/fphys.2018.01060

Tormos, Kathryn V., Anso, E., Hamanaka, Robert B., Eisenbart, J., Joseph, J., Kalyanaraman, B., & Chandel, Navdeep S. (2011). Mitochondrial Complex III ROS Regulate Adipocyte Differentiation. *Cell Metabolism, 14*(4), 537-544. doi:https://doi.org/10.1016/j.cmet.2011.08.007

Unamuno, X., Frühbeck, G., & Catalán, V. (2019). Adipose Tissue. In I. Huhtaniemi & L. Martini (Eds.), *Encyclopedia of Endocrine Diseases (Second Edition)* (pp. 370-384). Oxford: Academic Press.

van Dam, A. D., Boon, M. R., Berbée, J. F. P., Rensen, P. C. N., & van Harmelen, V. (2017). Targeting white, brown and perivascular adipose tissue in atherosclerosis development. *European Journal of Pharmacology, 816*, 82-92. doi:https://doi.org/10.1016/j.ejphar.2017.03.051

Vidal, P., & Stanford, K. I. (2020). Exercise-Induced Adaptations to Adipose Tissue Thermogenesis. *Front Endocrinol (Lausanne), 11*, 270. doi:10.3389/fendo.2020.00270

Villarroya, F., Cereijo, R., Villarroya, J., & Giralt, M. (2017). Brown adipose tissue as a secretory organ. *Nat Rev Endocrinol, 13*(1), 26-35. doi:10.1038/nrendo.2016.136

Wang, L., Xu, M., Qin, J., Lin, S. C., Lee, H. J., Tsai, S. Y., & Tsai, M. J. (2016). MPC1, a key gene in cancer metabolism, is regulated by COUPTFII in human prostate cancer. *Oncotarget, 7*(12), 14673-14683. doi:10.18632/oncotarget.7405

White, U., & Ravussin, E. (2019). Dynamics of adipose tissue turnover in human metabolic health and disease. *Diabetologia, 62*(1), 17-23. doi:10.1007/s00125-018-4732-x

Wilson-Fritch, L., Burkart, A., Bell, G., Mendelson, K., Leszyk, J., Nicoloro, S., . . . Corvera, S. (2003). Mitochondrial biogenesis and remodeling during adipogenesis and in response to the insulin sensitizer rosiglitazone. *Mol Cell Biol, 23*(3), 1085-1094. doi:10.1128/mcb.23.3.1085-1094.2003

Yoo, H. C., Park, S. J., Nam, M., Kang, J., Kim, K., Yeo, J. H., . . . Han, J. M. (2020). A Variant of SLC1A5 Is a Mitochondrial Glutamine Transporter for Metabolic Reprogramming in Cancer Cells. *Cell Metabolism, 31*(2), 267-283.e212. doi:https://doi.org/10.1016/j.cmet.2019.11.020

Yu, D., Shi, X., Meng, G., Chen, J., Yan, C., Jiang, Y., . . . Ding, Y. (2015). Kidney-type glutaminase (GLS1) is a biomarker for pathologic diagnosis and prognosis of

hepatocellular carcinoma. *Oncotarget, 6*(10), 7619-7631. doi:10.18632/oncotarget.3196

Zhang, Y., Marsboom, G., Toth, P. T., & Rehman, J. (2013). Mitochondrial respiration regulates adipogenic differentiation of human mesenchymal stem cells. *PLOS ONE, 8*(10), e77077. doi:10.1371/journal.pone.0077077

8 Supplementary figures

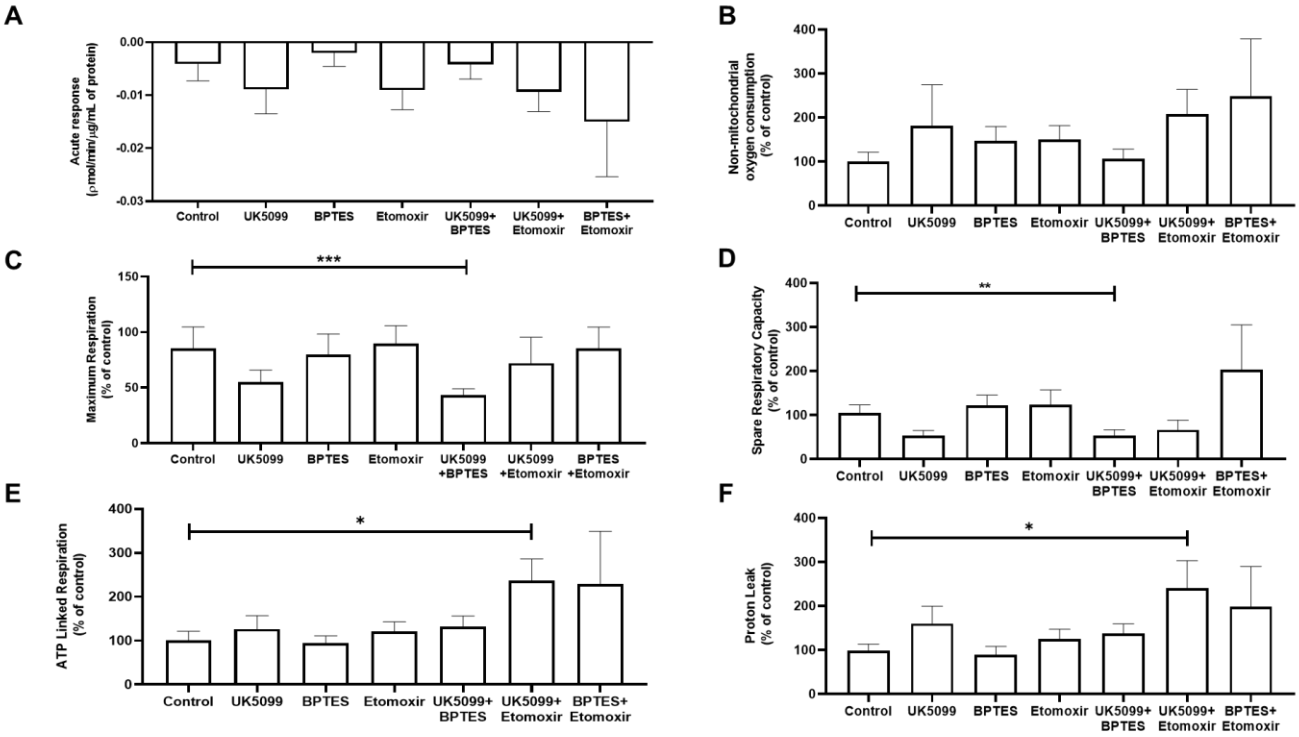

Supplementary Figure S1 - Influence of the inhibitors in (A) basal respiration (acute response); (B) non-mitochondrial oxygen consumption; (C) Maximum respiration oxygen consumption; (D) Spare respiratory capacity; (E) Proton Leak and (F) ATP link respiration in the VAT of patients with obesity. Except for the acute response, all values are normalized to the control group. (Friedman test * $p<0.05$, ** $p<0.01$, *** $p<0.001$).

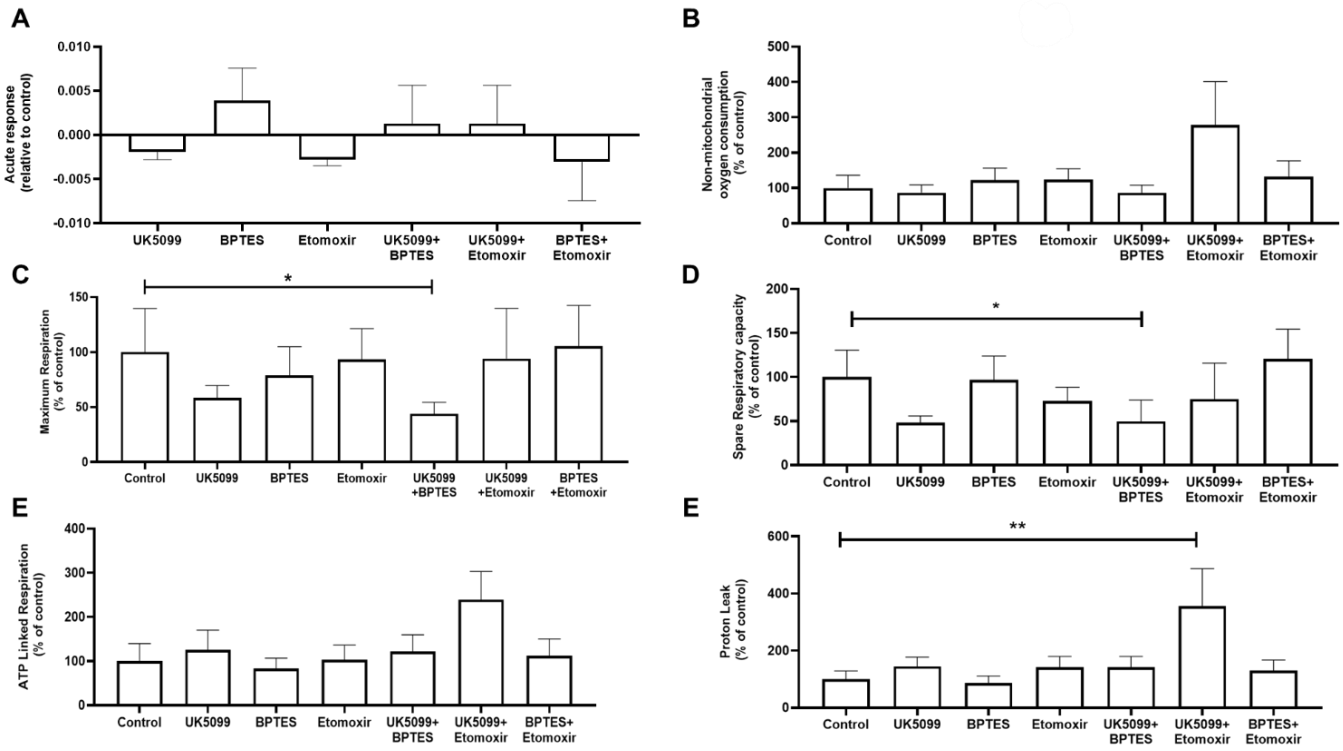

Supplementary Figure S2 - Influence of the inhibitors in (A) basal respiration (acute response); (B) non-mitochondrial oxygen consumption; (C) Maximum respiration oxygen consumption; (D) Spare respiratory capacity; (E) Proton Leak and (F) ATP link respiration in the VAT of patients with a BMI <40 kg/m^2. Except for the acute response, all values are normalized to the control group. (Friedman test *p<0.05, **p<0.01).

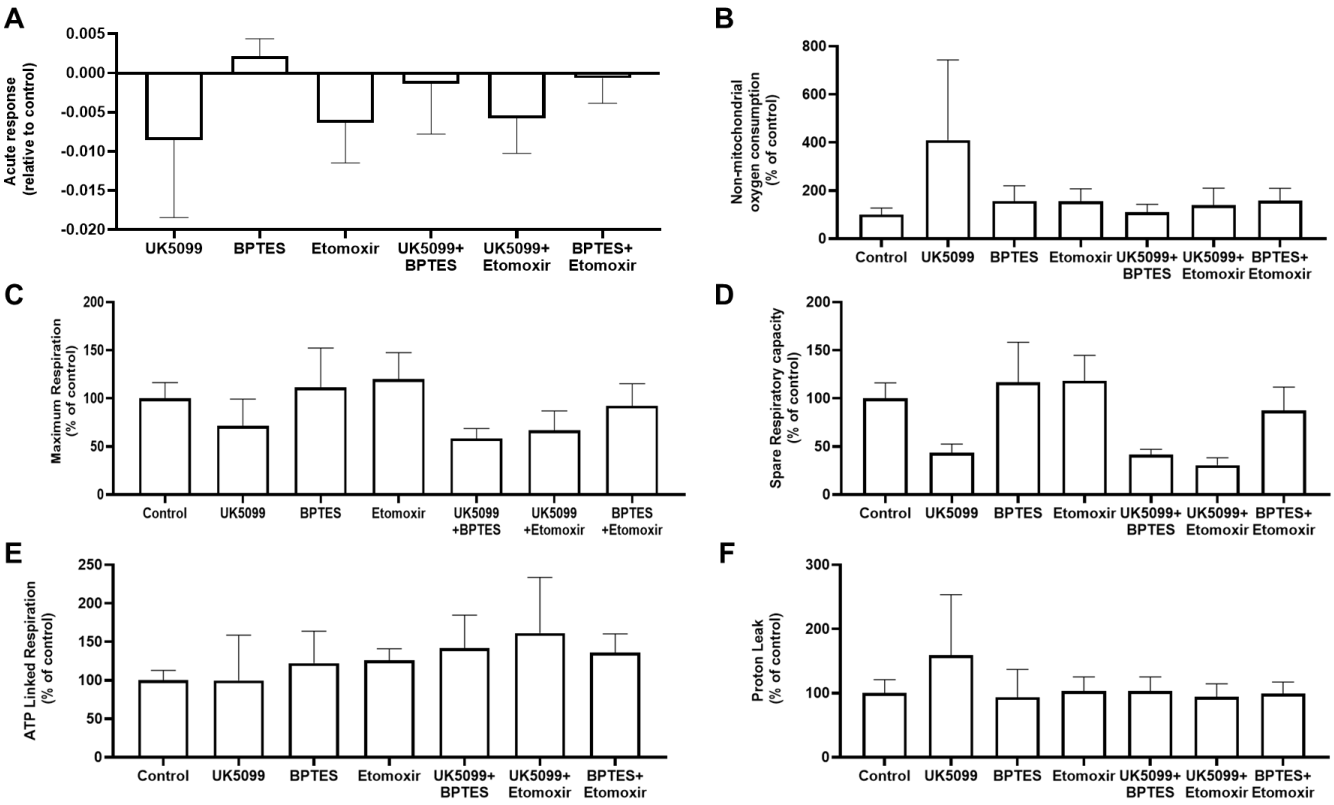

Supplementary Figure S3 - Influence of the inhibitors in (A) basal respiration (acute response); (B) non-mitochondrial oxygen consumption; (C) Maximum respiration oxygen consumption; (D) Spare respiratory capacity; (E) Proton Leak and (F) ATP link respiration in the VAT of patients with a BMI ≥40 kg/m^2. Except for the acute response, all values are normalized to the control group.

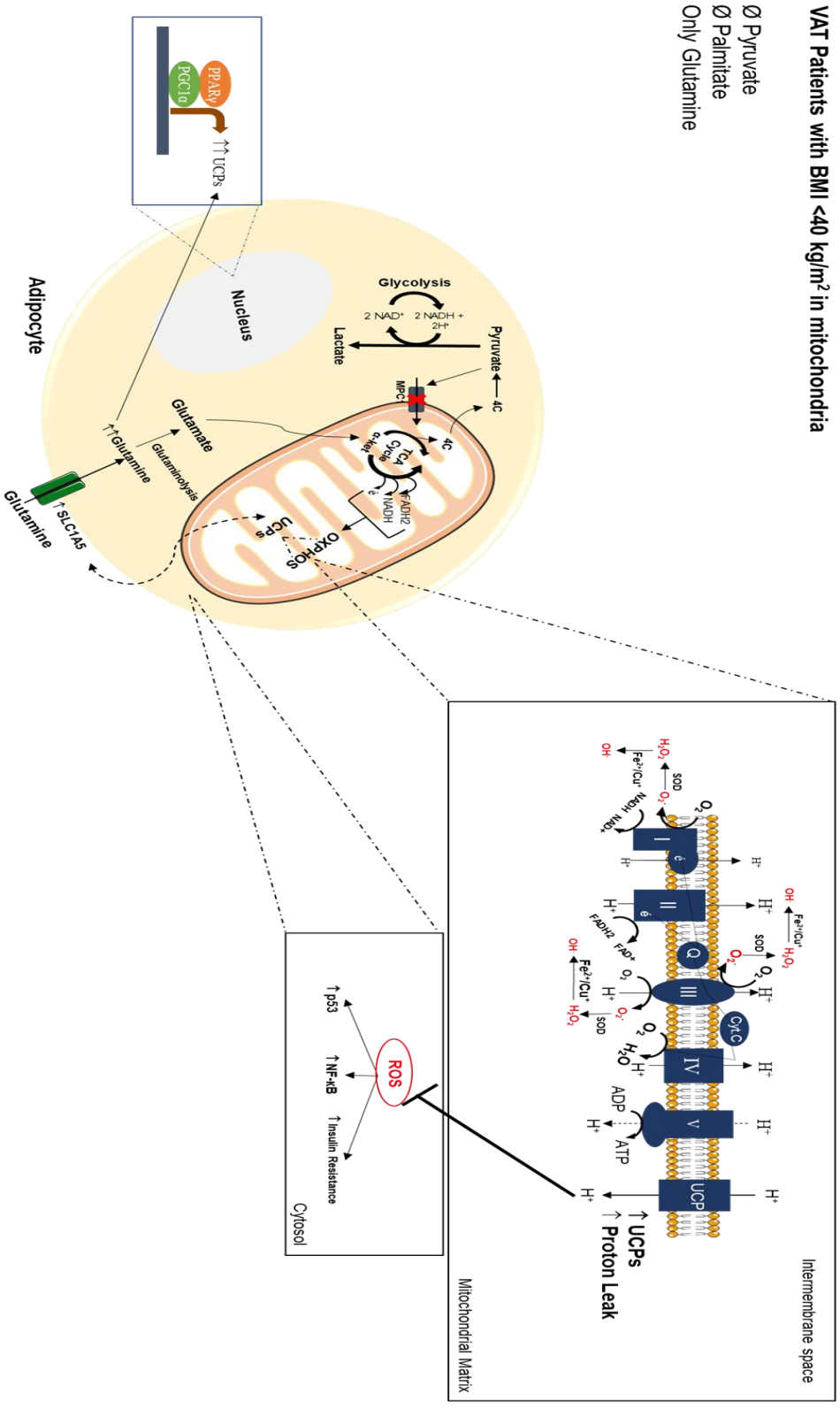

Supplementary Figure S4 - Possible role of glutamine in VAT of people with BMI <40 kg/m2. In the impossibility of pyruvate entering the mitochondria for further oxidative phosphorylation, glutamine is an efficient substrate used by cells to meet energy needs through glutaminolysis. In addition, we hypothesize that glutamine may increase the expression of UCPs, leading to an increase in proton leak and consequently to the inhibition of ROS production.